MICROWAVE MEASUREMENT OF SEMICONDUCTOR FILM CONDUCTIVITY

THE MICROWAVE MEASUREMENT OF THE CONDUCTIVITY OF A SEMICONDUCTING FILM

By

TONY MENG YUEN CHAN, B.ENG.

A Thesis

Submitted to the Faculty of Graduate Studies

in Partial Fulfilment of the Requirements

for the Degree

Master of Engineering

McMaster University

May 1964

MASTER OF ENGINEERING (1964) McMASTER UNIVERSITY
(Electrical Engineering) Hamilton, Ontario.

TITLE: The Microwave Measurement of the Conductivity of a Semiconducting Film.

AUTHOR: Tony Meng Yuen Chan, B.Eng. (McGill University)

SUPERVISOR: Professor M. W. Gunn

NUMBER OF PAGES: vii, 82

SCOPE AND CONTENTS: Indium-antimonide films have been prepared for experiments involving the application of high electric fields to this semiconducting material. The films have been deposited onto a mica substrate. To obtain high mobilities, a multilayer construction with subsequent annealing was used.

Measurements of the complex propagation coefficient of a section of waveguide containing the film have been made and the results agree closely with a numerical solution of a theoretical model proposed for the structure.

The design of a new type of a pulse generator for these high electric field experiments is described.

ABSTRACT

A sensitive microwave bridge has been assembled for the measurement of the complex propagation coefficient of a section of waveguide containing a semiconducting film. The bridge operating at a frequency of 9.25 Gc/s, can be balanced to one degree phase shift and 0.05 db attenuation.

Films of indium antimonide have been prepared by vacuum deposition onto mica substrates. A multilayer construction with subsequent annealing was used in an attempt to obtain high mobilities. Four n-type InSb films with thicknesses 2160 Å, 2180 Å, 4700 Å and 4800 Å were produced. The Hall Mobilities were found in the range between 500 to 1000 $cm^2/V\text{-}sec$.

Theoretical and numerical solutions of the complex propagation constant of a rectangular waveguide section containing a semiconducting film have been made. The analysis is based on the assumptions that the film thickness was negligible, the film surface was parallel to the narrow walls of the guide and that perfect electrical contact existed between the film and the broad walls of the guide.

Measurements of complex propagation coefficients have been carried out with the film mounted between mica sheets in a slotted waveguide in preparation for experiments involving the application of high electric d.c. fields to the sample. The measured complex propagation agreed closely with

the computed values confirming the validity of the theoretical model for this particular case.

The design of a new type of a pulse generator for these high electric field experiments is described. The pulse generator features a continuously variable pulse width from 0.2 μ sec. to 5 μ sec. with a low output impedance of approximately 13 ohms and a repetition rate adjustable to 1, 2, 5 and 10 pulses per second.

ACKNOWLEDGEMENTS

The author wishes to express his gratitude for the continued advice and encouragement received from Dr. M. W. Gunn. For a summer grant and most of the microwave instruments which made this investigation possible the author is deeply indebted to the Defence Research Board of Canada. The author is also grateful to Dr. C. K. Campbell for the facilities of the vacuum instrument in his low temperature laboratory.

TABLE OF CONTENTS

INTRODUCTION

This thesis describes the first stage of an investigation into the changes produced in the complex permittivities of semi-conductors, measured at microwave frequencies under conditions of high electric fields. At the microwave frequency the important parameter controlling the propagation is the differential carrier mobility $(\frac{dv}{d\varepsilon})$, if it is assumed that the microwave electric field is very much less than the applied electric field and that these two field vectors are parallel[1]. The change in $\frac{dv}{d\varepsilon}$ can be large, for example in n-type germanium $\frac{dv}{d\varepsilon}$ falls to zero in the range 4.5 to 9 kV/cm[2] and under such conditions the germanium offers zero impedance to a wave propagating through it. The effect has possible applications to microwave modulators operating in the nanosecond range[3] and also provides additional experimental information for the theory of conduction in semiconductors.

This thesis describes the design and assembly of equipment suitable for making measurements on films of indium-antimonide at a frequency of 9.25 Gc/s. A frequency in X band was chosen to avoid the complication of frequency dependent effects which for example become apparent in n-type germanium at 34.75 Gc/s[4]. However measurements in this band have the practical difficulty that samples several centimeters in length and width are required for insertion into the waveguide. Bulk material of such dimensions is difficult to obtain and it was

decided to carry out measurements on deposited thin films, in the first instance. The use of films has the advantages that physically large samples can be readily produced and that the propagation equations of the inhomogeneously filled waveguide section are simplified, compared with the guides loaded with thick samples of semiconductor. Also they are particularly suitable for measurements on high conductivity semiconductors as they fulfil the requirement that the sample thickness be very much less than the skin depth. In recent years a great deal of effort has been devoted to the preparation of thin samples of semiconducting materials and to investigations of their properties. Such films have been used in many Hall-effect devices[5][6] and more generally in infra-red application[7]. Moreover, work on very thin films has been done to examine the surface structure of solid materials[8].

The use of a thin film also enables high conductivity semiconductors to be investigated without introducing too high an attenuation over the section of guide carrying the film and indium antimonide was chosen for the initial experiments. Up to the present, changes in the conductivity of this material have been measured by measuring the change in resistance of samples with increasing fields[9][10]. The microwave method of measurement used in this project gives a sensitive means of measuring the changes produced by increasing electric field as the differential mobility is measured rather than the mobility. Also measurements at a microwave frequency enables information on frequency dependent effects in the material to be obtained. Measurements of these effects must be carried out under pulsed conditions to

avoid joule heating of the sample and a typical pulse duration is 0.5 μsec with a repetition rate of 1 p.s. It is desirable that the pulse generator should have a low output impedance to be able to feed samples of widely differing characteristics and also it should produce perfect rectangular pulses. The complex permittivity can be measured on a microwave bridge which can be operated under pulsed condition, the sample being inserted in one arm of such a bridge.

The equipment required for the above measurements comprises a pulse generator, a microwave bridge and thin indium antimonide films together with theoretical and numerical solutions of a film-loaded waveguide. These matters are discussed separately in the following four chapters.

CHAPTER I

The Thyratron On-Off Pulse Generator

Although this thesis is concerned with a new design of a pulse generator, the Thyratron On-Off pulse generator, two other main types of pulse generator, namely the Line-type and the Hard-tube pulse generator[11] will be described briefly to compare the general approaches.

Requirements for a pulse generator are:

(i) A pulse as truly rectangular as obtainable,

(ii) The pulse length and repetition rate variable over as wide a range as possible, particularly if this can be done continuously.

(iii) The pulse magnitude variable to about 20 Kv.

(iv) An output impedance suitable for load resistances of 50 ohms and higher.

Main types of pulse generators

(A) Line-type pulse generator.

The operation of a line-type pulse generator depends on the discharge of a charged transmission line into a matched load. The schematic circuit diagram of this type of pulse generator is shown in Figure 1-1.

If the transmission line is charged to a voltage V and is assumed to be lossless, the output current is[12]

$$I(s) = \frac{V/s}{R_L + Z \coth \delta s}$$

where δ is the one-way transmission time of the line, and Z is its characteristic impedance.

The inverse Laplace Transform gives the output current as

$$i(t) = \frac{V}{Z + R_L}\left\{1 - u(t - 2\delta) - \frac{Z - R_L}{Z + R_L}\left[u(t - 2\delta) - u(t - 4\delta)\right] + \left(\frac{Z - R_L}{Z + R_L}\right)^2\left[u(t - 4\delta) - u(t - 6\delta)\right] ----\right\}$$

The derivation is found in Appendix A.

where $U(\Delta t)$ is a step function as

$U(\Delta t) = 1$ for $\Delta t > 0$

$U(\Delta t) = 0$ for $\Delta t < 0$

$\Delta t = (t - n\delta)$ $\quad n = 2, 4, 6, \ldots$

Thus for a matched load $R_L = Z$ the output current consists of a single rectangular pulse of magnitude $I = \frac{V}{2Z}$ and duration $\tau = 2\delta$. If the output is measured across the load R_L, a single rectangular pulse of magnitude $\frac{V}{2}$ will be obtained.

Normally, a coaxial cable is used for the transmission line and has a signal velocity of about 500 ft/μ sec.[13] A cable length of 250 feet is thus required to produce a 1 μ sec. output pulse.

Since the above analysis is based upon a lossless transmission line, the actual output pulse shape is not perfectly rectangular. The ripples on the flat top of the pulse rapidly increase in magnitude as the pulse amplitude rises above 5 Kv.[14] Furthermore, the load impedance of the line-type pulse generator is fixed in order to match the characteristic impedance of the transmission line. Above all, the greatest disadvantage of a line-type pulse generator is that whenever the width of the pulse is desired to be varied, the length of the transmission line will have to be altered, which can only be done by switching to other individual transmission lines with different lengths. Also, the maximum magnitude of the output pulse is only one half of the supply voltage V as mentioned above.

(B) Hard-tube pulse generator.

A hard-tube pulse generator is actually a class C amplifier whose coupling capacitor is used as an energy reservoir. The time interval during which the high-vacuum tube is conducted can be controlled by the application of the proper voltage to the grid and essentially, it determines the pulse duration.

Figure 1-2 is a simplified form of a hard-tube pulse generator with a triode as the switching tube.

For the present discussion the storage capacitor is considered to be charged to a voltage V_w, which is very nearly equal to $E_{bb'}$ the power supply voltage. It is further assumed that the capacitance of C_w is so large that the change in voltage during a pulse is negligibly small. The circuit can be represented as shown in Figure 1-3 by replacing the

charged capacitor C_w by a battery of voltage V_w.

The tube can be represented by its characteristic resistance r_p and an ideal switch S_T. In this equivalent circuit the capacitor C_s has been introduced to represent the shunt capacitance, which is the sum of the capacitances of the load, the switch tube and that due to the circuit wiring.

If the conduction period is t_1, i.e. the switch S_T is closed at $t = 0$ and opened at $t = t_1$, a nearly rectangular pulse shape will be obtained across the load R_L with a magnitude equal to V_w which is approximately equal to E_{bb} as shown in Figure 1-4, where R_1 is the effective resistance of r_p and R_L in parallel.

The pulse shape shown in Figure 4 is produced when the conduction period t_1 is much greater than both time constant, R_1C_s and R_LC_s.

This type of pulse generator produced a better rectangular pulse than the line-type pulse generator. However its efficiency is lower than the line-type pulser as it requires more cathode-heating power and greater power to drive it. For example, a hard-tube pulse generator with a pulse-power output of 3 Mw has been built with a 35 Kv power supply, whereas for a line-type pulse generator the same power output is obtained with only about 14 Kv from the power supply if a standard 50-ohm load is used.[15] The other disadvantage is that the load resistance must necessarily be high, in the order of kilohms, because of the effective resistance of the tube during conduction. (100 ohms for 5D21) Hence it is not suitable for feeding low impedance loads.

The Thyratron On-Off pulse generator

This generator design seeks to combine the advantages of both the above circuits in that it can provide continuously variable width pulses into both high and low resistance loads.

Basic Circuit

The Thyratron On-Off pulse generator is based on a pulse-forming circuit discussed by Edwards.[16]

If a step voltage is applied to a resistive load, R, at time $t = 0$ by means of a switch T_1 and at time $t = t_1$ it is shorted by means of another switch T_2, the output waveform across the load R_L will theoretically be a rectangular pulse shape as shown in Figure 1-5. The resistance in the circuit is to limit the current as T_2 is closed. The duration of the pulse is t_1 and this may be continuously varied over a wide range of values by adjustment of t_1.

Requirements of switched T_1 and T_2 to be met are:

(i) Very short switching-on period.

(ii) The associated inductance and capacitance as small as possible.

(iii) Can stand large peak current through it during conduction.

(iv) Almost short-circuited (very low impedance) during conduction.

Switches

The hydrogen thyratrons 5C22 were used as switches T_1 and T_2 in Figure 1-5. This type of tube is designed to work with a 50 ohm load and has a peak voltage plate of 16 Kv and a peak plate current of 325 amp.

It requires zero grid bias and a minimum trigger voltage +150 V. No published data are available on the impedance of the tube during conduction but the major capacitance - the grid-anode capacitance, and the inductance between anode and cathode have been measured as 15 pf and 2 μh at 1 Mc/s.

The filament transformers.

The tube requires 6 V, 10 amp filament supply. The filament transformer of the tube T_1 requires a primary-secondary insulation suitable for 16 Kv and the secondary winding comprises 35 turns of No. 12 A.W.G. enamelled copper wire onto a common filament transformer with a primary winding. This construction gives a primary-secondary capacitance of about 35 pf.

Pulse-Forming Circuit analysis.

This analysis is based on the equivalent circuit of the pulse-forming circuit in Figure 1-5 is shown in Figure 1-6, where r_1, L_1, C_1 and r_2, L_2, C_2 are the equivalent elements of the tubes T_1 and T_2, and r is chosen to be 11 ohm. The capacitor C' represents the sum of the stray capacitance of the tube and the primary-secondary winding capacitance of the filament transformer of the tube T_1. This equivalent circuit can be simplified further as shown in Figure 1-7 for C_1 and C_2 C'. The complete shape of the output pulse across the load R_L is determined in the following three steps:

(i) Rise time -- the switch T_1 is closed at t = 0 and V(t) is evaluated over the time interval 0 t t_1. The output voltage across R_L is

$$V(t)\Big|_{0 \leq t \ll t_1} = \frac{VR_L}{r + r_1 + R_L}\left[1 - e^{-\alpha t}\left(\frac{\alpha}{\beta}\sin \beta t + \cos \beta t\right)\right] \quad ---(A)$$

$$\text{where } \alpha = \frac{r + r_1}{2L} + \frac{1}{2R_L C'}$$

$$\beta = \sqrt{\frac{r + r_1 + R_L}{L_1 C' R_L} - \alpha^2}$$

the derivation can be found in Appendix B. A computer programme has been written in Appendix C to calculate V(t) in Equation (A).

(ii) Pulse top --- the time interval between $0 \leq t \leq t_1$.

If $t \gg \frac{1}{\alpha}$, the term $e^{-\alpha t}$ in equation (A) tends to zero and the output waveform in this part becomes

$$V(t)\Big|_{0 < t < t_1} = \frac{VR_L}{r + r_1 + R_L} \qquad ----------(B)$$

Actually it is not a straight line as given in equation (B), but it falls expontentially with a time constant $(r + r_1 + R_L)C$ which is much greater than t_1, if a charging capacitor C is used instead of the battery V in Figure 1-5.

(iii) Decay time --- the switch T_2 is closed at $t = t_1$ and V(t) is evaluated for $t \geq t_1$.

As the lower tube is closed the voltage across the load R_L drops rapidly to $V\left(\frac{r_2}{r_1 + r_2 + r}\right)$, then decays expontentially with the time

constant $(r_1 + r_2 + r)C$. Hence,

$$V(t)\Big|_{t \geq t_1} = V\left(\frac{r_2}{r_1 + r_2 + r}\right) e^{-\frac{t - t_1}{(r_1 + r_2 + r)C}} \qquad \text{-----(C)}$$

A pulse with a long tail is obtained as shown in Figure 1-8.

If the resistance r increases, the tail will start lower, but the magnitude of the output pulse will be decreased as shown by equations (B) and (C). This is not desirable as a large part of energy is lost in the resistor r. The decay time of the tail can be less if the capacitance C is decreased. However, it will cause the top-part to sag as a consequence.

Improvement of the main pulse generator.

If instead of the series tube T_2, another thyratron T_3 is connected in parallel across the capacitor C, as in Figure 1-9(a), the decay time constant can be reduced from $(r + r_1 + r_2)C$ to r_3C, which is only about 1/7 of the value if T_2 is used. However, the pulse will then begin falling exponentially after T_3 is fired as shown in Figure 1-9(b).

The exponential decay of the pulse after T_3 is fired is much smaller than if T_3 is omitted. The tail of the decaying pulse is only 3 μ sec. long even if a 0.5 μf charging capacitor is used.

This pulse shape thus obtained does not have the required sharp trailing edge. Furthermore, the current through T_3 will exceed its peak current specification. In order to enable the fall time to be shorter, both thyratrons T_2 and T_3 are needed, T_2 being in series with T_1

while T_3 being in parallel with the charging capacitor C. A typical value of 1 MΩ for the charging resistor R_c is used for a pulse per sec. output. This improved circuit is shown in Figure 1-10.

The three tubes operation then consists of the following steps:

(i) T_1 is fired at t = 0 to produce a step output across the load resistance R_L.

(ii) After T_1 is fired the pulse form will be maintained at its peak value until $t = t_1$ when T_2 is fired. The pulse shape will drop instantaneously to 1/7 of the peak value.

(iii) As soon as the peak value drops to 1/7 T_3 is fired, which makes the pulse shape fall exponentially.

Layout of the main pulse generator.

The layout of the generator is shown in Figure 1-11. The Thyratrons are operated in a horizontal position and care has been taken to keep all leads as short and direct as possible. To prevent high voltage flashover and to allow heat radiation air spacing of at least $1\frac{1}{2}$ in. are required and the charging resistor is screened with a polythene cylinder. Insulated stands are required for the mounting of the bases of the thyratrons.

X-Ray Shielding.

The operation of hydrogen thyratrons involves the risk of X-ray radiation. To avoid this the entire assembly is covered by a metal cabinet $14\frac{3}{8} \times 18\frac{1}{8}$ in. with $10\frac{3}{8}$ in. height.

The driver stage.

The three thyratrons in the main pulse generator circuit are triggered by three gas tubes (2D21) which are controlled by a simple pulser through different delay controls of integrating circuits. It is shown in Figure 1-12. A pulse transformer, which has high voltage insulation suitable for 20 Kv, must be used at the grid of the upper tube T_1 for its cathode is floating at a voltage equaltothe magnitude of the output pulse during conduction. The operation of T_1 and T_2 and T_3 from a single trigger tube proved to be unsatisfactory. When triggered directly by three different integrating circuits they fail to fire properly due to low grid-cathode impedance, and produced considerable "jitter" in the output pulse duration. The grid circuit of V_2 controls its firing point and hence controls T_2. Therefore it controls the pulse duration. The grid circuit of V_3 controls the tail shape of the pulse. These two with the variable coil at the anode of the tube T_1, which controls the rise time, determine the output pulse shape.

The repetition rate of pulses is controlled by a multivibrator.

The output pulse duration is continuously variable from $0._2$ μ sec. to 5 μ sec. and by adjustment of the timing and other relevant circuits pulse duration of several hundred μ sec. can be obtained.

The trigger pulse transformer.

The only requirement of this 400 V 1:1 ratio pulse transformer is that it has a primary-secondary winding insulation suitable for 20 Kv.

In order to produce a faster rise-time a ferrite-core is used.

For a source resistance of 200 Ω and a secondary load of 1.2 KΩ, a transformer of the following specifications proved satisfactory:

Core : Philips D45/39 ferrite core

Primary : 150 turns of 30 A.W.G. enamelled copper wire wound in 3 layers.

Secondary: same winding as primary with 4 layers of 1/4 mm polythene sheeting giving an insulation for 30 Kv.

Primary L : 0.9 mH at 1 Kc/s

Secondary L : 0.8 mH at 1 Kc/s

Primary-Secondary C = 15 pf

Pictures in Figure 1-15, 1-17 and 1-18 are taken by a "DuMont" Oscilloscope camera type 353 with 3000 ASA Polaroid films from a type 585 Oscilloscope shown in Figure 1-14.

In the driver stage the firing of the second 2D21 gas tube is delayed by the variable resistance (50 KΩ) and the capacitor 100 pf, similarly for the firing of the third 2D21 gas tube. This would at most be delayed by 5 μsec., but if the 100 pf capacitor be replaced by one with higher value, a longer delayed time could be obtained. The anode-grid capacitors in the multivibrator control its repetition rate consequently the repetition rate of the pulse generator.

Theoretical Results for Pulse Rise Time
(obtained from Computer 7040 programme I)

Time (μ sec)	V = 4 Kv, r = 11 Ω, r_1 = 2 Ω and L_1 = 2 μh					
	C' = 50 pf			C' = 200 pf		
	R_L = 66Ω	R_L = 200Ω	R_L = 1 KΩ	R_L = 66Ω	R_L = 200Ω	R_L = 1 KΩ
0.00	0. volt	0. volt	0. volt	0. volt	0. volt	0. volt
0.05	3342.	3983.	3654.	2966.	4733.	6117.
0.10	3342.	3765.	4915.	3419.	3845.	3565.
0.15	3342.	3754.	4299.	3343.	3491.	3190.
0.20	3342.	3756.	3790.	3340.	3924.	5077.
0.25	3342.	3756.	3811.	3342.	3692.	3020.
0.30	3342.	3756.	3952.	3342.	3766.	4430.
0.35	3342.	3756.	3986.	3342.	3762.	3893.
0.40	3342.	3756.	3958.	3342.	3749.	3745.
0.45	3342.	3756.	3941.	3342.	3759.	4225.
0.50	3342.	3756.	3944.	3342.	3755.	3731.
0.55	3342.	3756.	3949.	3342.	3756.	4054.
0.60	3342.	3756.	3950.	3342.	3756.	3944.
0.65	3342.	3756.	3949.	3342.	3756.	3895.
0.70	3342.	3756.	3948.	3342.	3756.	4016.
0.75	3342.	3756.	3949.	3342.	3756.	3898.
0.80	3342.	3756.	3949.	3342.	3756.	3972.
0.85	3342.	3756.	3949.	3342.	3756.	3950.
0.90	3342.	3756.	3949.	3342.	3756.	3935.
0.95	3342.	3756.	3949.	3342.	3756.	3965.
1.00	3342.	3756.	3949.	3342.		3937.

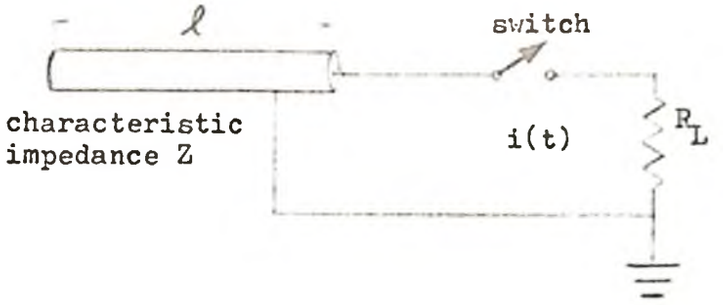

FIGURE 1-1

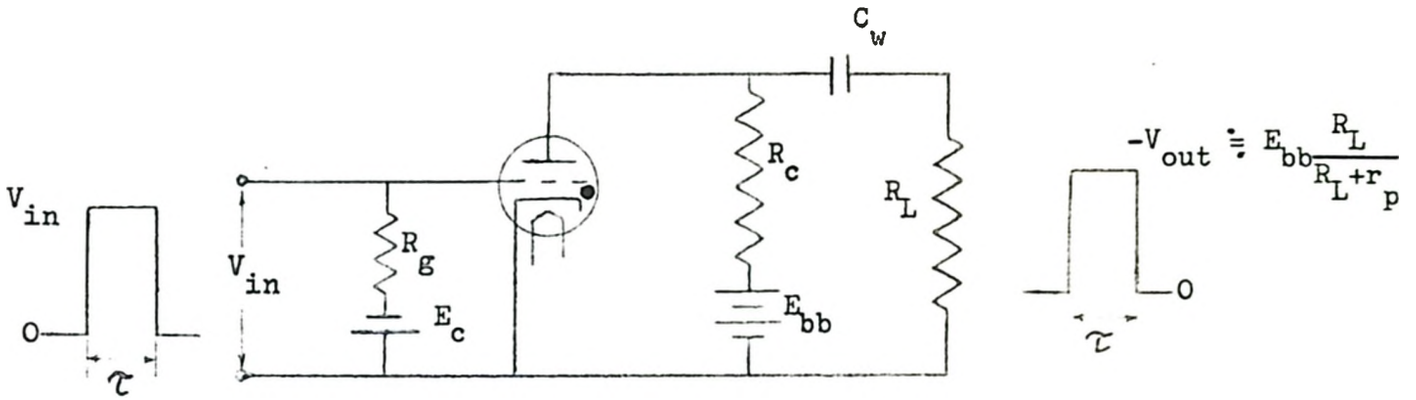

FIGURE 1-2

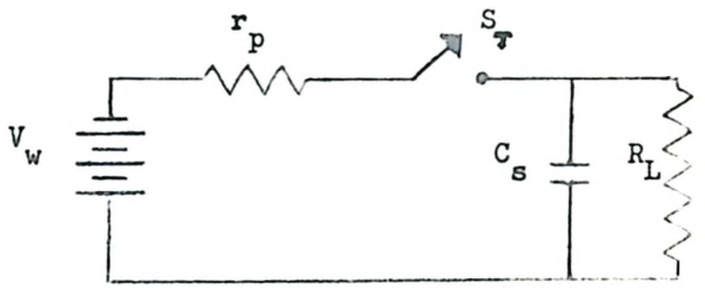

FIGURE 1-3

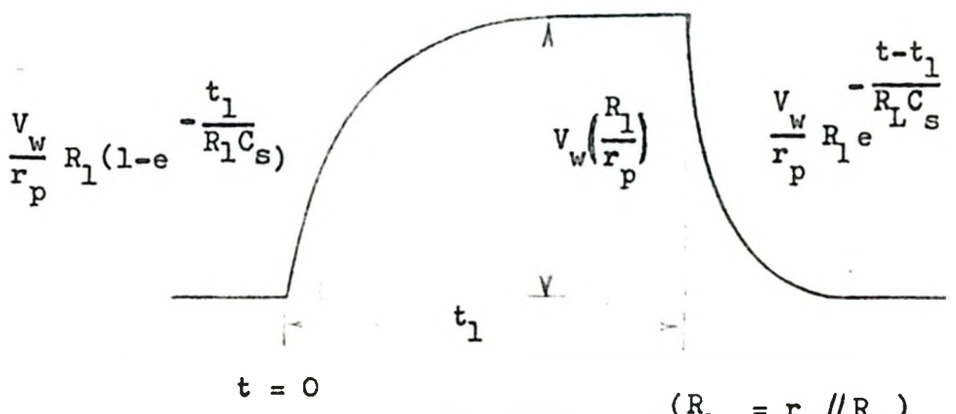

FIGURE 1-4 $(R_1 = r_p // R_L)$

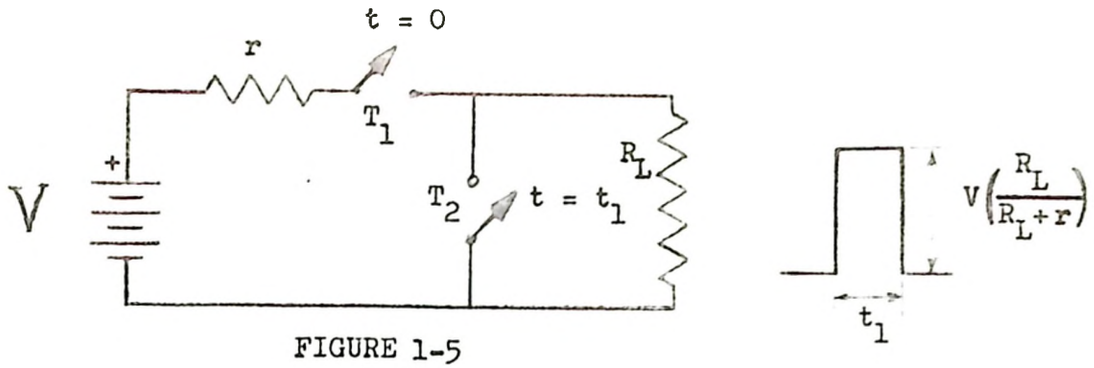

FIGURE 1-5

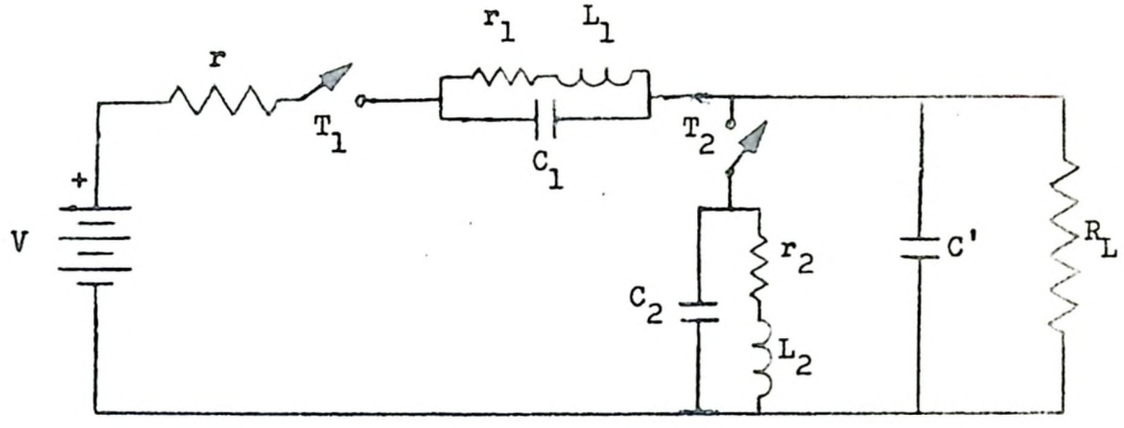

FIGURE 1-6

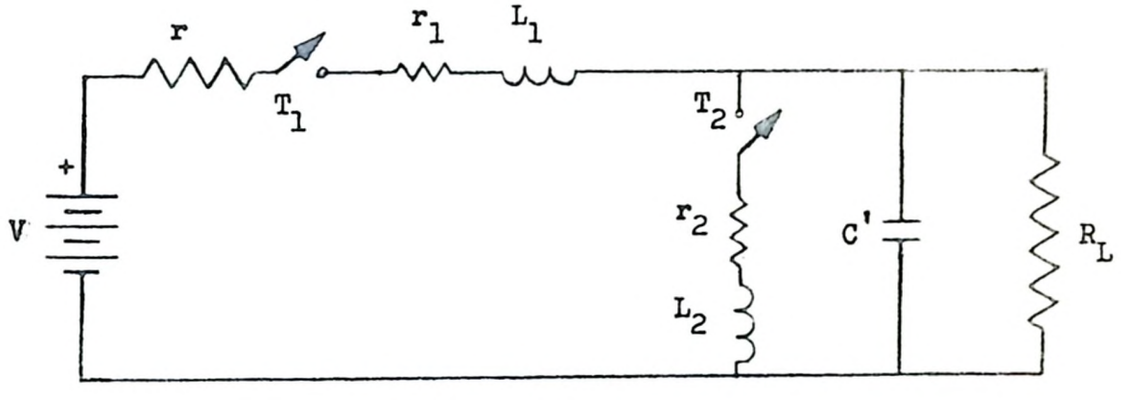

FIGURE 1-7

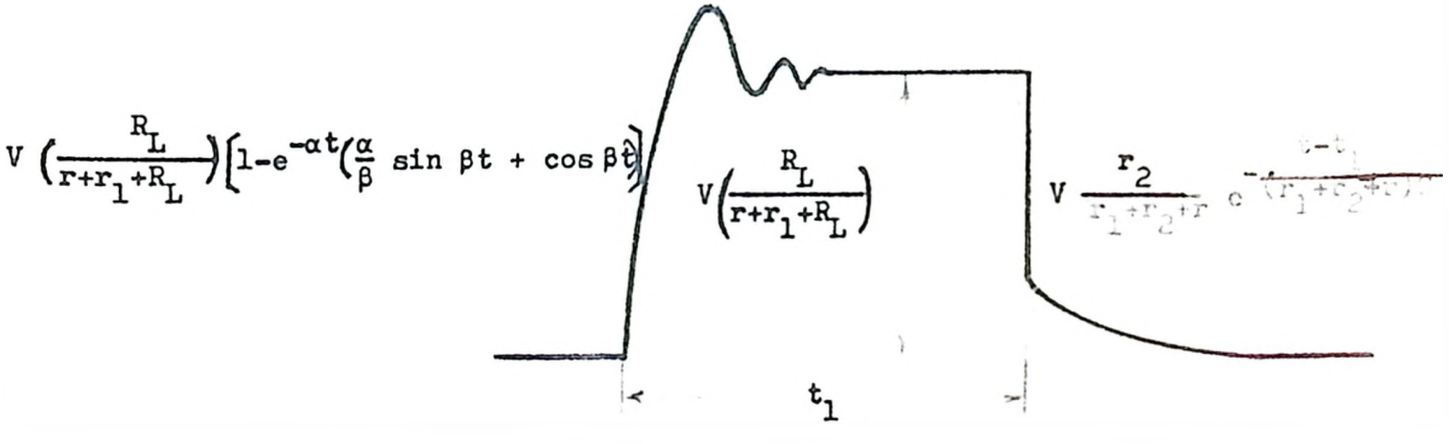

FIGURE 1-8

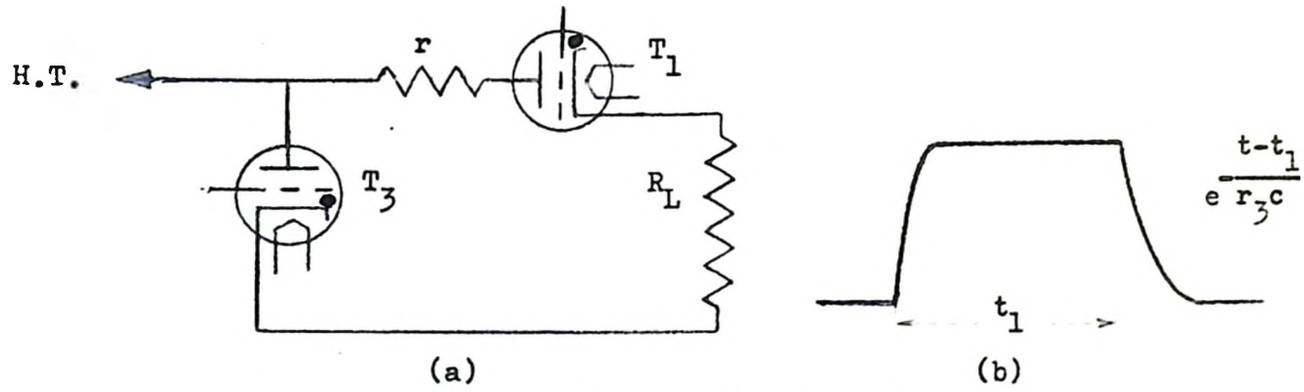

FIGURE 1-9 ($r_3 \ll R_L$ and r

C refers to Figure 1-10

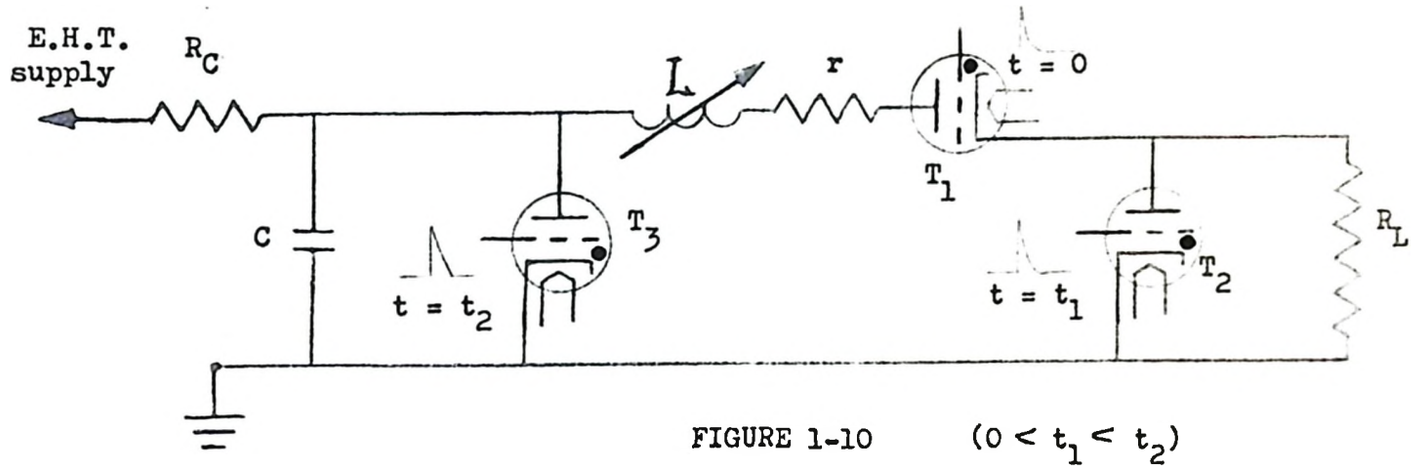

FIGURE 1-10 ($0 < t_1 < t_2$)

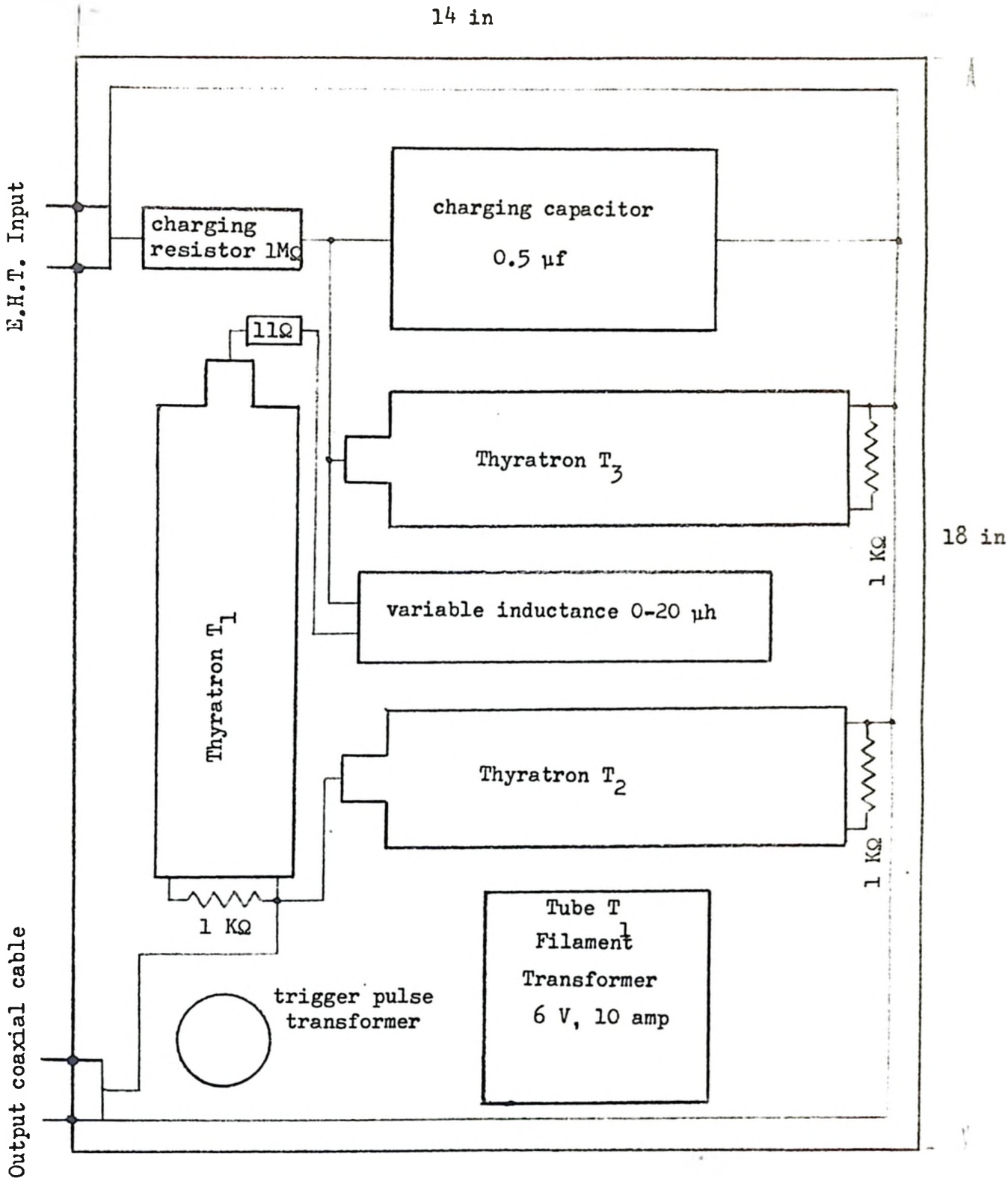

FIGURE 1-11 Layout of the Generator
(Multivibrator and filament transformers for Tubes T_2 and T_3 beneath chassis)

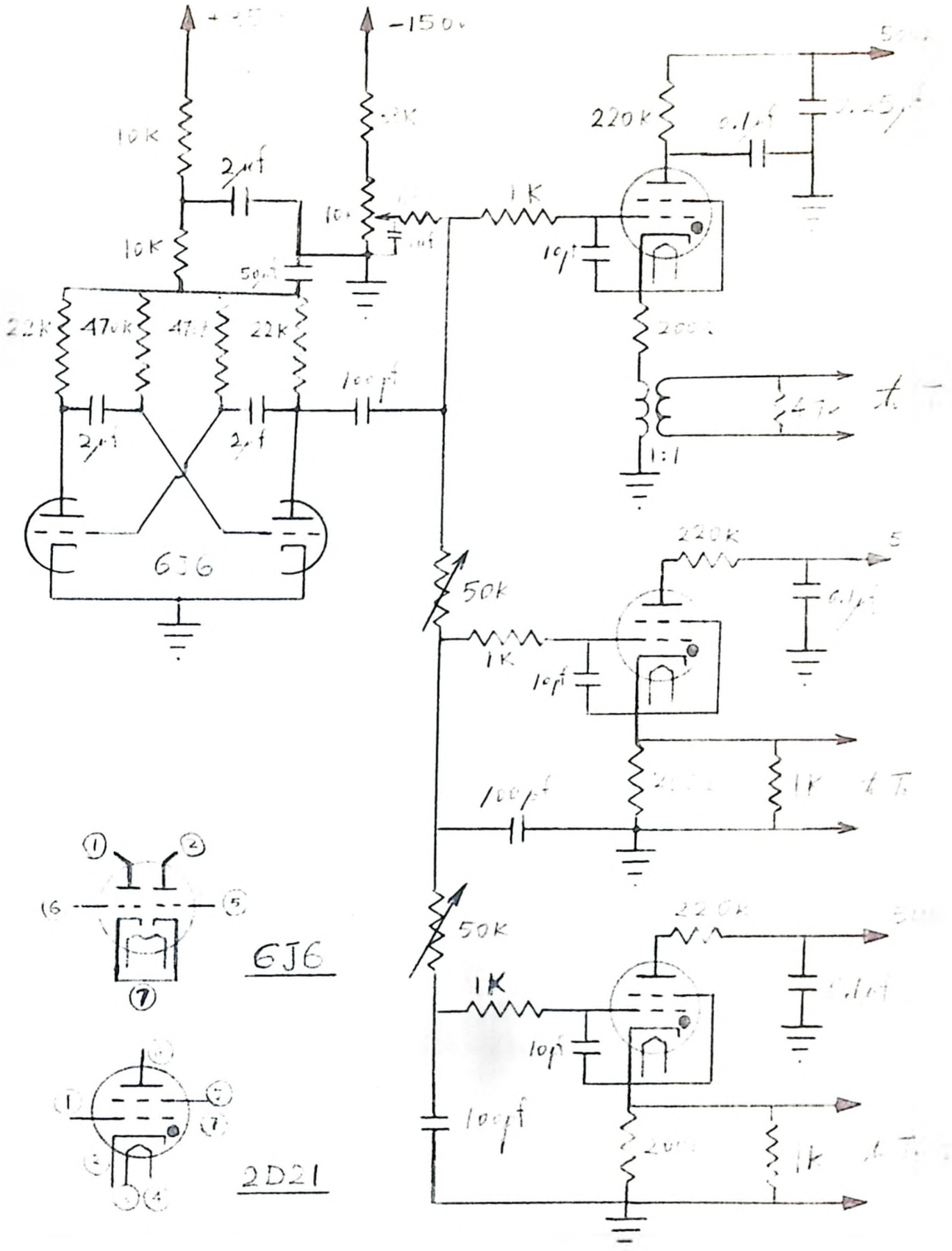

FIGURE 1-12 The driver stage

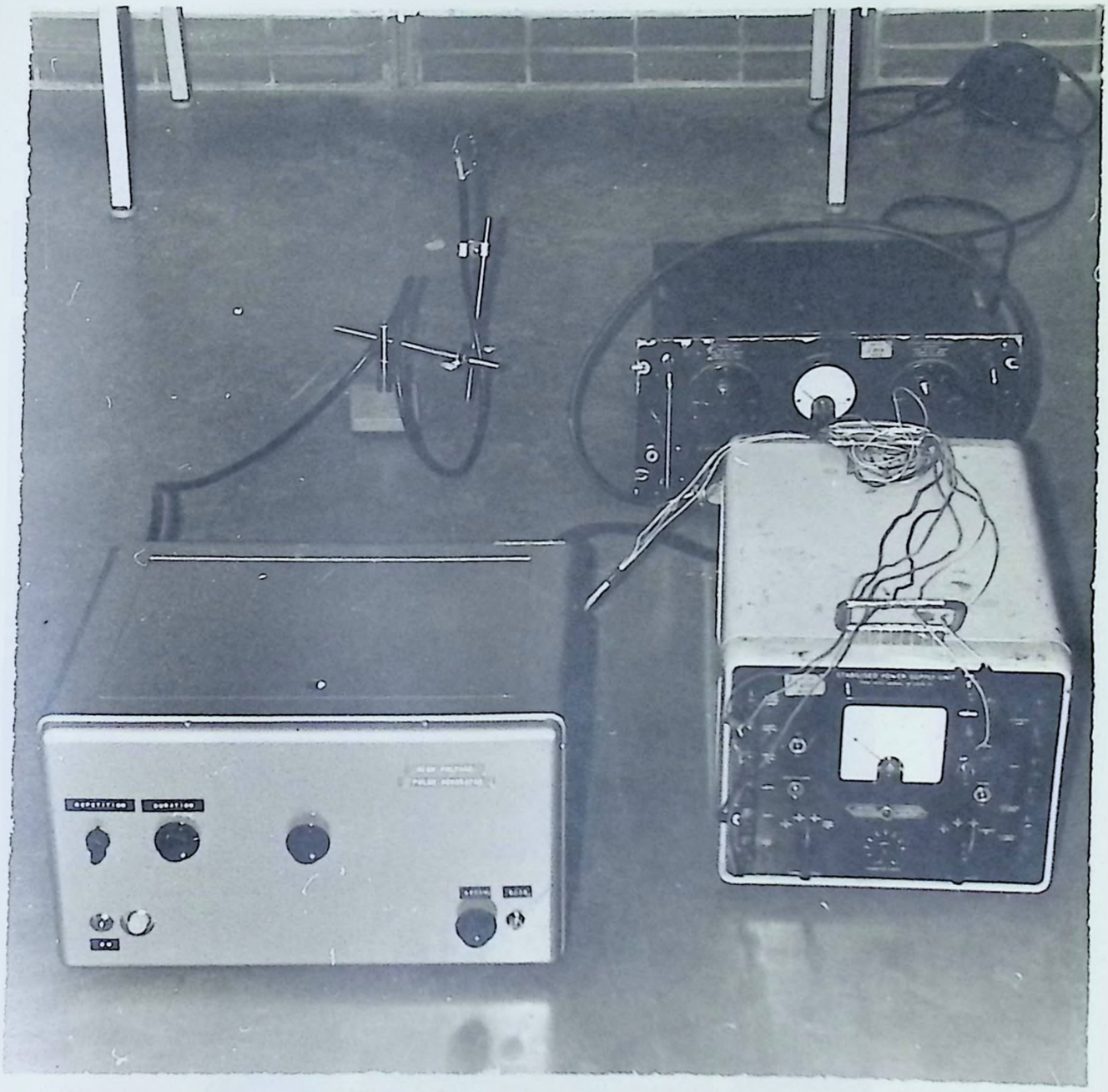

Thyratron On-Off Pulse Generator.

H.H.T. Power Supply.

Driver stage Power Supply.

FIGURE 1-13

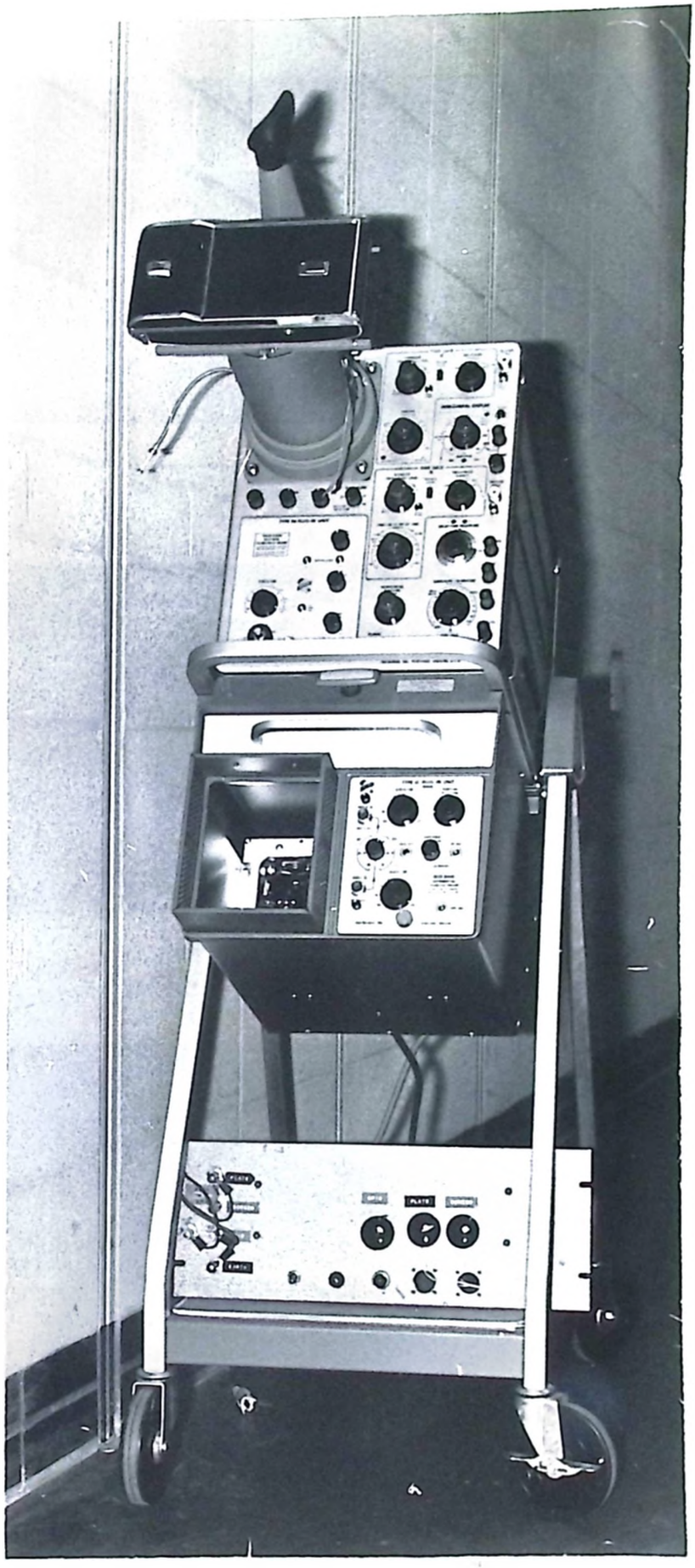

FIGURE 1-14 Oscilloscope Type 585

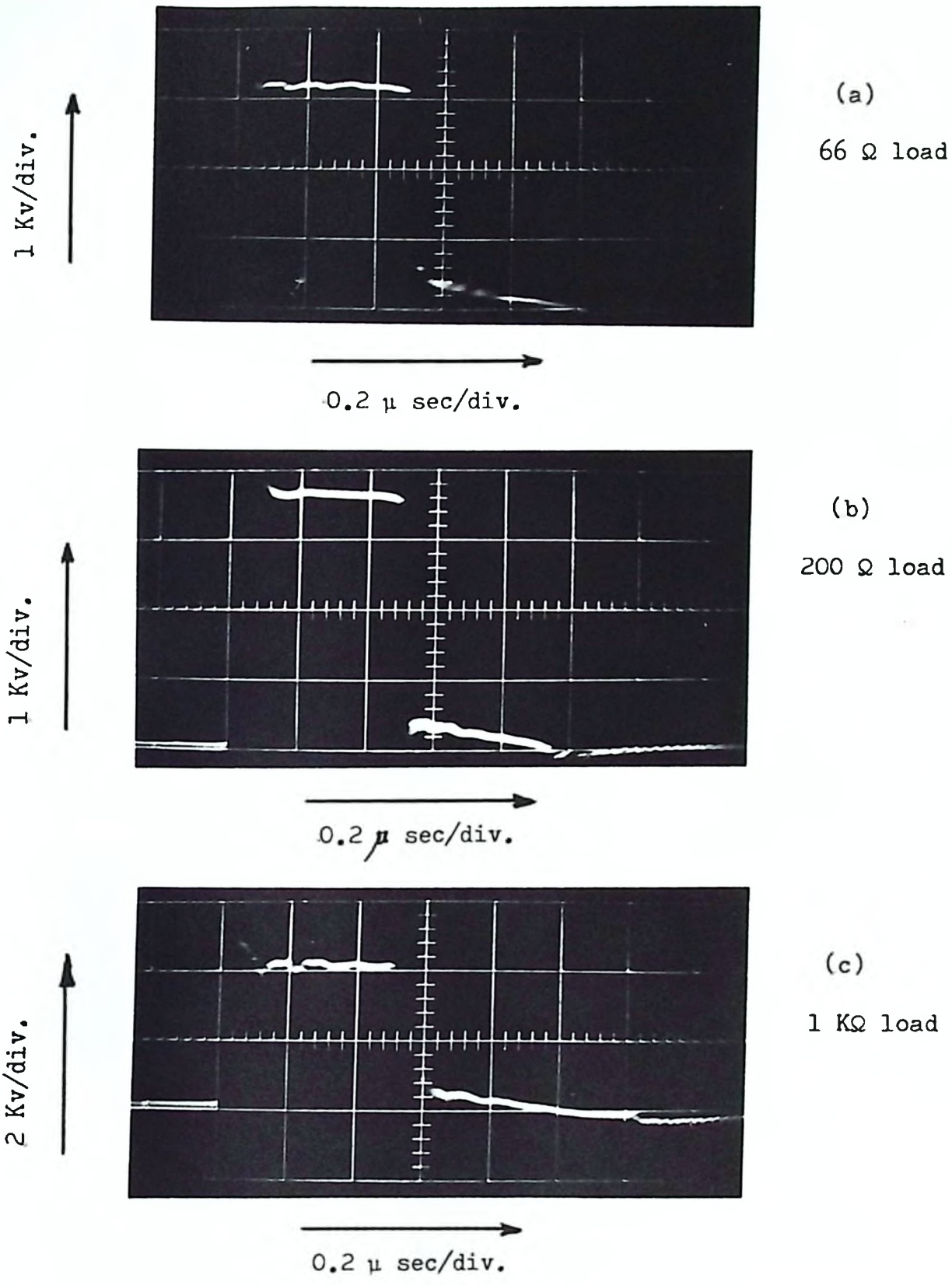

FIGURE 1-15 Output Pulses of the Thyratron On-Off Pulse Generator (variable anode inductance L = 0)

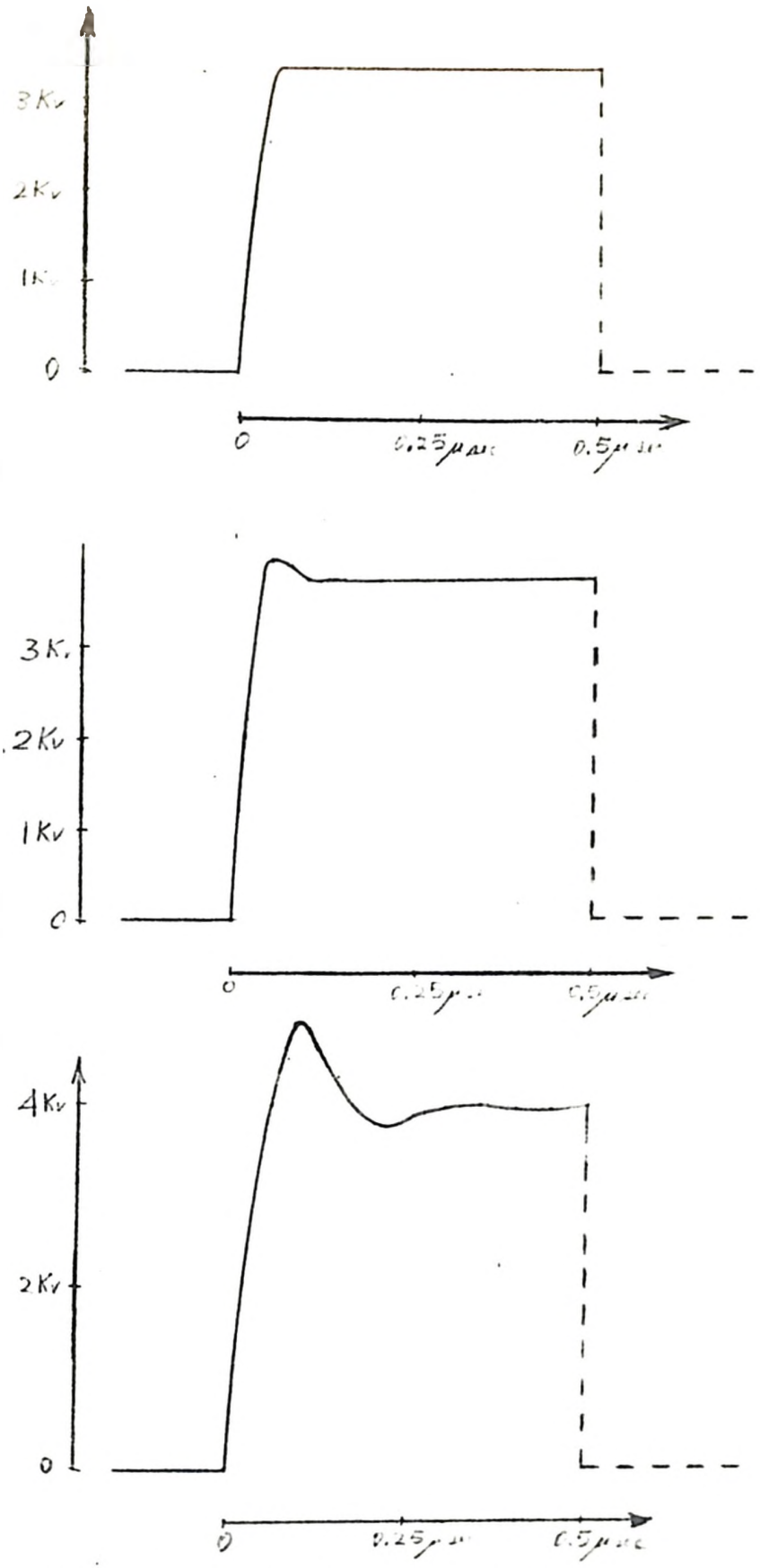

FIGURE 1-16 Theoretical Output Pulses
Rise Time with L_1 = 2 μh and C' = 50 pf.
(variable anode inductance L = 0)

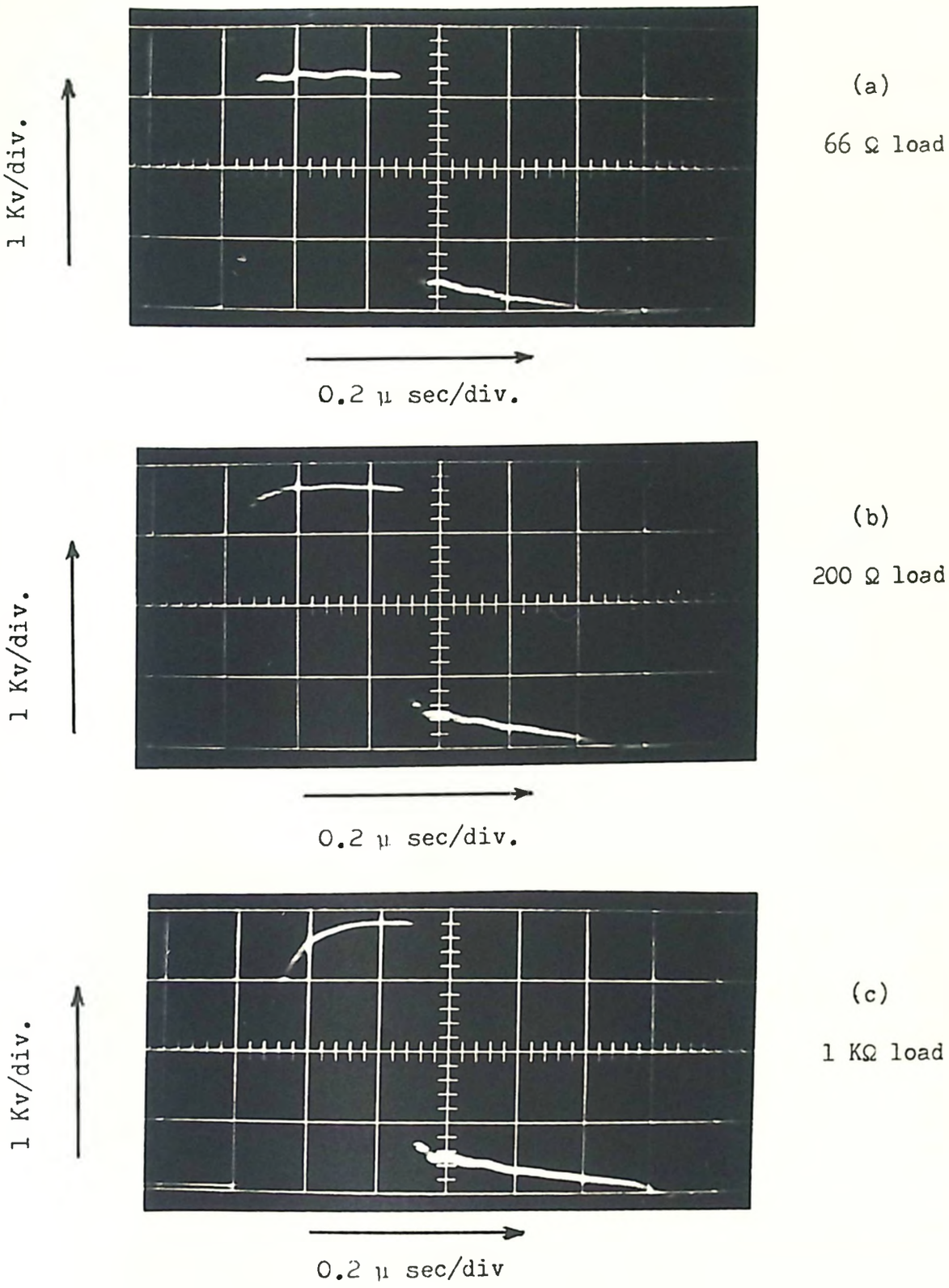

FIGURE 1-17 Typical Output Pulses with 6.5 ft. long RG 8 A/U coaxial cable (29.5 pf/ft) by adjusting the variable anode inductance L.

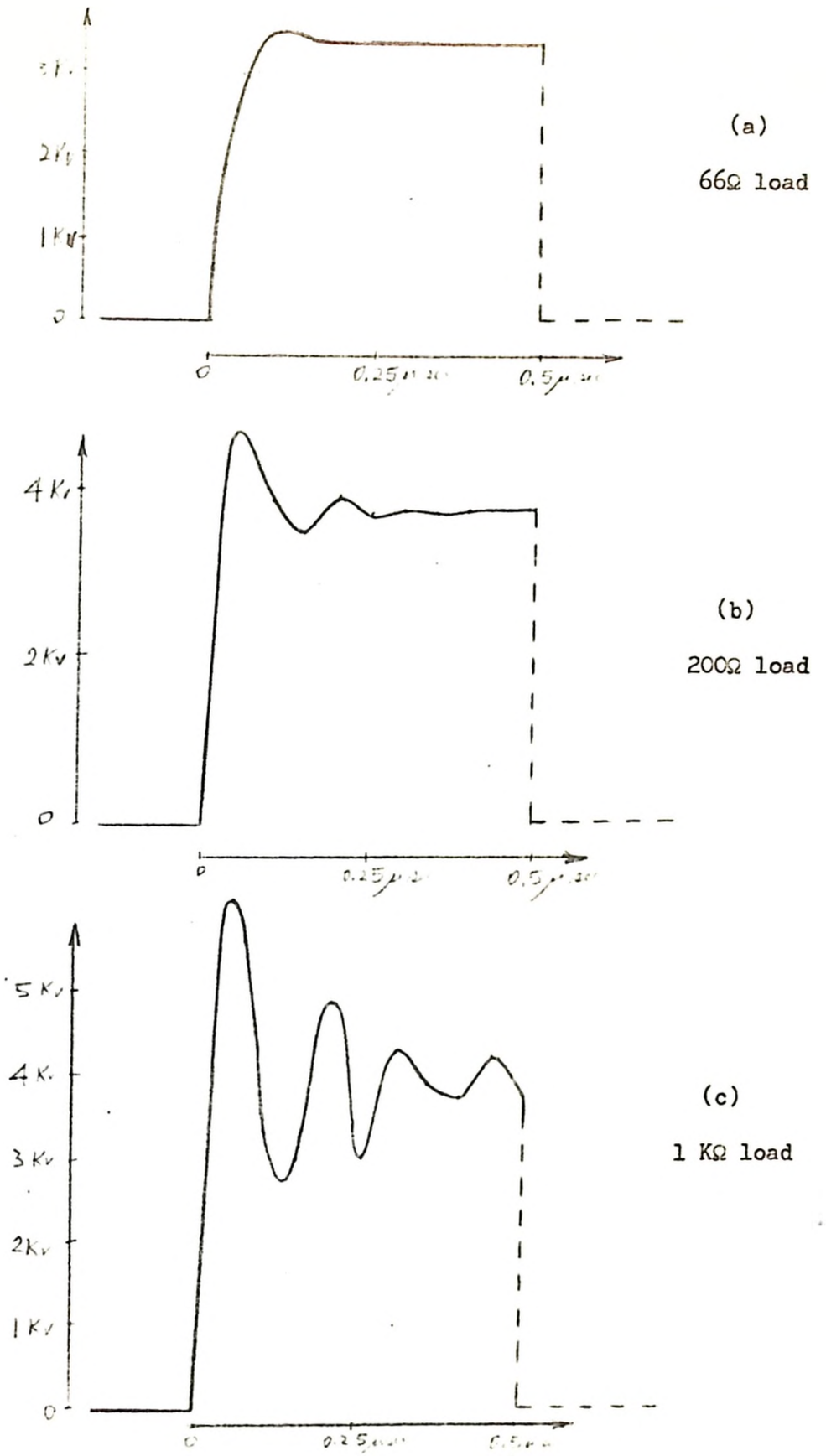

FIGURE 1-19 Theoretical Output Pulse with 6.5 ft. long RG 8 A/U coaxial cable (29.5 pf/ft.) (variable anode inductance L = 0)

Discussion

The measured 4 Kv, 0.5 μ sec. pulses with different loads are very close to the theoretical solution and confirm the validity of the theoretical model discussed in Appendix B. The pulse shape is very convenient for measurements as the top is flat and the trailing corner is very sharp.

Figure 1-15 shows measured pulse shapes with 66Ω, 200Ω and 1 KΩ loads. Comparison with the theoretical "Rise time" curves in Figure 1-16 confirms the measured values of (1) the major capacitance (grid-anode) of the Thyratron 15 μf, (2) the primary-secondary capacitance of the tube T_1 filament transformer, 35 pf, and also (3) the inductance of the Thyratron between anode and cathode, 2 μh which were used in the theoretical model. From the voltage ratios of the starting point of the pulse tail to the pulse top, the resistance of the Thyratron during conduction, is found to be 2.36Ω.

Figure 1-17 shows typical output pulses without overshoot for 66Ω, 200Ω and 1 KΩ.

Figure 1-18 shows the effect of the charging capacitance C for 66Ω load. The sag of the "Pulse top" becomes apparent if an 0.1 μf capacitor is used. However the Pulse generator needs more input power as the charging capacitance is increased.

CHAPTER II

The Preparation of Indium Antimonide Films

General Consideration

Semi-conducting films have been prepared by the following methods:

1) Lapping down a slice of the solid material.

2) Suddenly squashing a drop of molten material.

3) Vacuum deposition and subsequent annealing.

The film obtained by lapping has the same Hall Mobility as the bulk material. However, by this technique, it is difficult to obtain a film of thickness less than the skin depth of indium antimonide at microwave frequency. The skin depth for indium antimonide of conductivity $2.5 \times 10^{4} \mho m^{-1}$ is calculated to be $\delta = \frac{1}{\pi f \mu_o \sigma}$ (17) $= 3.31 \times 10^{-5} m$ at 9.25 Gc/s.

Bate and Taylor[18] have described the second method of producing thin indium antimonide films. The apparatus for preparation of the layers consisted essentially of a heated quartz substrate on which rested the piece of indium antimonide ($\frac{1}{10}$ g.). A second (cold) quartz substrate with a weight (a heavy brass rod) above it was dropped from a height of about 3 cm. onto the molten indium antimonide which then squashed into a thin layer between the two flats. The heater current

was switched off immediately the weight was released and the whole assembly allowed to cool to room temperature before the apparatus was opened. Films 10μ thick of 1 cm^2 area were obtained in above way. However, because of different thermal expansion coefficients of indium antimonide and the substrate material, the final layer was either cracked in the case of quartz flats or buckled in the case of soda glass flats. Although the thin layers prepared were polycrystalline, their electrical and optical properties were in good agreement with the single crystal material from which they were obtained. The highest Electron Mobility obtained was 2.38×10^4 cm^2/v-sec for n-type layer. This is quite close to the mobility of bulk material, 70,000 cm^2/V sec.(19)

Paparoditis(20) has prepared films, 200 - 1700 Å thick, of n-type indium antimonide by evaporation in a high vacuum followed by annealing in argon at temperature varying between 150° and 350°C. The maximum values of resistivity and Hall coefficient occurred when annealing temperatures between 200°C and 300°C were used. Paparoditis seems to have assumed that indium antimonide distils over homogeneously when evaporated in a vacuum giving at once a film of indium antimonide. Calculation from his published curves relating Hall coefficient and conductivity shows that his optimum value for the mobility was 75 cm^2/V-sec for a film 700 - 780 Å thick. This is much lower than that of the bulk material.

Dale and Senecal(21) found carrier concentrations lie between 6×10^{15} and $4 \times 10^{19}/cm^3$ and Hall mobilities between 10 and 500 cm^2/V-sec

for evaporated InSb films of 550 to 3750 Å thick. The mobility increases with increasing annealing temperature over most of the range from 100 to 500°C.

Evaporated InSb films are characterized, as a rule, by extremely low mobility. Kurov and Pinsker[22] report hole mobilities only between 2 and 8 cm^2/V-sec. Lanney and Colombani[23][24] report maximum electron mobilities of about 500 and 1000 cm^2/V-sec. respectively.

Presnov and Synorov[25] evaporated Indium and antimony separately and simultaneously on to a glass slide in a vacuum. For a film 4000Å thick they obtained a value of 50 cm^2/V-sec. for the Hall mobility. Günther[26] used the same technique and obtained electron mobility of the order of 10^4 cm^2/V-sec. in InAs and InSb films grown by the simultaneous evaporation of the individual constituents, at controlled rate, onto a heated substrate. The highest value he obtained is 13000 cm^2/V-sec. with substrate temperature at about 700°C and annealing temperature near 100°C.

Koike and Barlow[27] found that when InSb is heated in a vacuum it separates, in a vapour phase, into its two components. Thus the film is not indium antimonide but indium and antimony in almost distinct layers. They produced a multi-layer film by depositing a very small quantity of InSb at a time and annealing it at intervals. These films were found to have a mobility of more than 3000 cm^2/V-sec. The highest value obtained being 19000 cm^2/V-sec. for the 5 x 10 mm specimen. They state that "indium is quite volatile and its volatilization which is effected by the impurity concentration is related to the mobility of the film produced".

Experimental Work

The films used in the present experiment were prepared by a vacuum deposition technique.

The bulk material used was n-type InSb with an impurity concentration of $1.9 \times 10^{16}/cm^3$ and mobility of 6.6×10^4 $cm^2/V\text{-sec}$. at room temperature. The bulk material was first cut down to about 15 mg. pieces. Sheets of mica measuring about 2 mils thick were used as substrates. All of these were first cleaned by carbon tetrachloride and then washing in boiling distilled water separately. They were finally dried in an oven at a temperature near 200°C immediately before being placed inside the evaporation apparatus, the "Speedivac" Coating Unit, Model 12E3. The vacuum chamber was cleaned by means of the ion-bombardment process and the substrate was heated to 200°C - 250°C before the first layer, 15 mg., was deposited. Following this deposition the substrate was then annealed at a temperature of 200°C - 250°C for an hour. Additional layers were then deposited by repeating the same procedures. Films were prepared containing 4 and 8 layers. The evaporation procedure was carried out at a pressure of 5×10^{-6} Torr or greater (1 Tor = 1 mm Hg). Films obtained in this way can be assumed to have a uniform thickness and a multi-layer film is probably formed.[27]

Calculation of the thickness of the film.

If the material arrives at a small area on a surface inclined at an angle Θ to the direction of the vapour stream which has an angle ϕ from the vertical and assume that the evaporation takes place according

to Knudsen's law, the thickness of a film deposited is given by[28]

$$t = \frac{m}{\pi\rho} \quad \frac{\cos\phi \ \cos\theta}{r^2}$$

where m is the mass of the material evaporated, r is the distance from the material to the substrate, and ρ is the density of the material (5.7 g/cm^3 for indium antimonide).[15]

A number of films were produced and their properties were examined.

The Hall coefficients of In-Sb films are measured by conventional method as shown in the following schematic diagram.

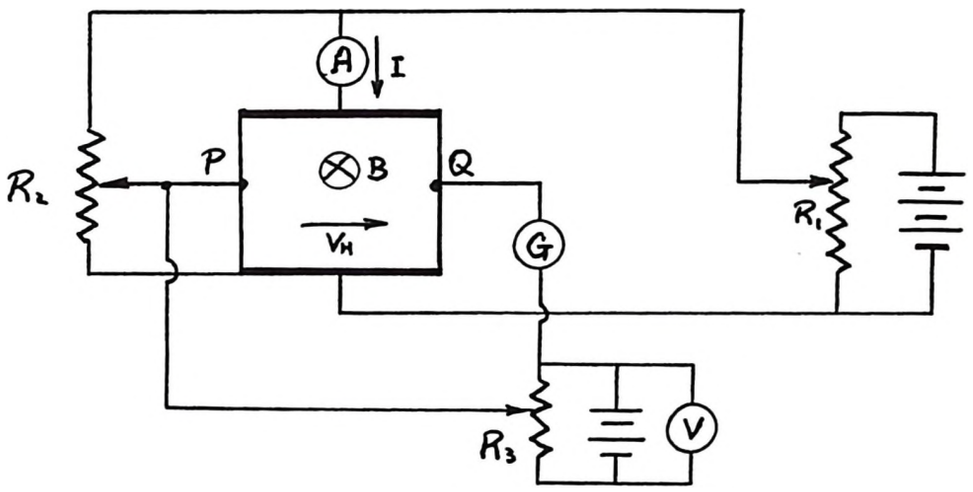

The magnetic induction density B is directed perpendicularly into the paper. R_1 controls the current I. R_2 is the compensating resistance for the asymmetric contacts. The Hall voltage V_H is balanced by R_3. All of them are Kelvin Varley Voltage Dividers. (G) is a Cambridge spot Galvanometer, No. L-357473. Two indium strips are deposited onto the InSb film serve as contacts. Points P and Q are indium soldered.

Sample Calculations

(A) Thickness of Sample II InSb films

$m = 59.2$ mg

$\rho = 5.7$ g/cm^3

$r = 11.94$ cm

$\phi = 14.1^\circ$

$\theta = 14.1^\circ$

the thickness of the film,

$$t = \frac{m}{\pi\rho} \quad \frac{\cos\phi \cos\theta}{r^2}$$

$$= \frac{59.2 \times 10^{-3}\text{g.}}{5.7\ \pi\ \text{g/cm}^3} \times \frac{(\cos 14.1^\circ)(\cos 14.1^\circ)}{(11.94)^2\ \text{cm}^2}$$

$$= 2.18 \times 10^{-5}\ \text{cm.}$$

$$= 2180\ \text{Å}$$

(B) Hall Mobility and Electron Concentration of Sample II InSb film.

$t = 2180 \times 10^{-10}$ m

$\sigma = \frac{1}{Rt} = 4950\ \mho\text{-m}^{-1}$

$\frac{V_H}{BI} = 3.88 \times 10^{-3}$ V/amp-gauss

$= 3.88$ m^2/coul.

If the ratio of the length to breath of the specimen exceed 4[36]

the Hall Coefficient $R_H = \frac{V_H}{BI} t$

$$= 38.8 \times 2180 \times 10^{-10}$$

$$= 8.45 \times 10^{-6} \text{ m}^3/\text{coul.}$$

In the general case of a rectangular specimen the measured value of R_H is related to the theoretical value by a shape factor. For a square specimen this equals 0.7.

the true Hall Coefficient $R_{H(true)} = R_H/0.7$

$$= 12.1 \times 10^{-6} \text{ m}^3/\text{coul.}$$

the Electron Mobility $\mu_n = \frac{8}{3\pi} \sigma R_{H(true)}$

$$= \frac{8}{3\pi} \times 4950 \times 12.1 \times 10^{-6}$$

$$= 509 \times 10^{-4} \text{ m}^2/\text{V-sec.}$$

the Electron Concentration $n = \frac{\sigma}{\mu_n e}$

$$= \frac{4950}{509 \times 10^{-4} \times 1.6 \times 10^{-19}}$$

$$= 6.09 \times 10^{23} \ 1/\text{m}^3$$

the Hall Mobility $\mu_H = \sigma R_{H(true)}$

$$= 4950 \times 12.1 \times 10^{-6}$$

$$= 600 \times 10^{-4} \text{ m}^2/\text{V-sec.}$$

Results

(I) Thicknesses and resistances of InSb films

Samples	I	II	III	IV
No. of layers evaporated mass, m	4 122.3 mg	4 59.2 mg	4 59.2 mg	8 119.9 mg
ø	0°	14.1°	15°	0°
e	0°	14.1°	15°	0°
r	11.94 cm	11.94 cm	11.94 cm	11.94 cm
thickness, t	4800 Å	2180 Å	2160 Å	4700 Å
dimension	3.6cm X 2.75cm	3.6cm X2.7cm	3.6cm X 2.7cm	4.7cm X2.95cm
resistance (measured)	1.05 KΩ	695Ω	635Ω	260Ω
resistance per square, R	1.375 KΩ	926Ω	846Ω	414Ω
conductivity, σ	1515 $\mho$-m^{-1}	4950 $\mho$-m^{-1}	5460 $\mho$-m^{-1}	5140 $\mho$-m^{-1}

II Hall Mobilities and Electron Concentration of InSb films

Sample	I	II	IV	Units
thickness, t	4800	2180	4700	Å
mean value of $\frac{V_H}{BI}$	6.65×10^{-3}	3.88×10^{-3}	3.05×10^{-3}	$V/_{amp\text{-}gauss}$
Hall Coefficient, R_H	31.95×10^{-6}	8.45×10^{-6}	14.3×10^{-6}	m^3/coul.
True Hall Coefficient $R_{H(true)}$	45.6×10^{-6}	12.1×10^{-6}	20.5×10^{-6}	m^3/coul.
Electron Mobility, μH	654×10^{-4}	509×10^{-4}	948×10^{-4}	m^2/V-sec.
Electron concentration, n	1.545×10^{23}	6.09×10^{23}	3.45×10^{23}	$1/_{m^3}$
Hall Mobility μ_H	770×10^{-4}	600×10^{-4}	1116×10^{-4}	m^2/V-sec

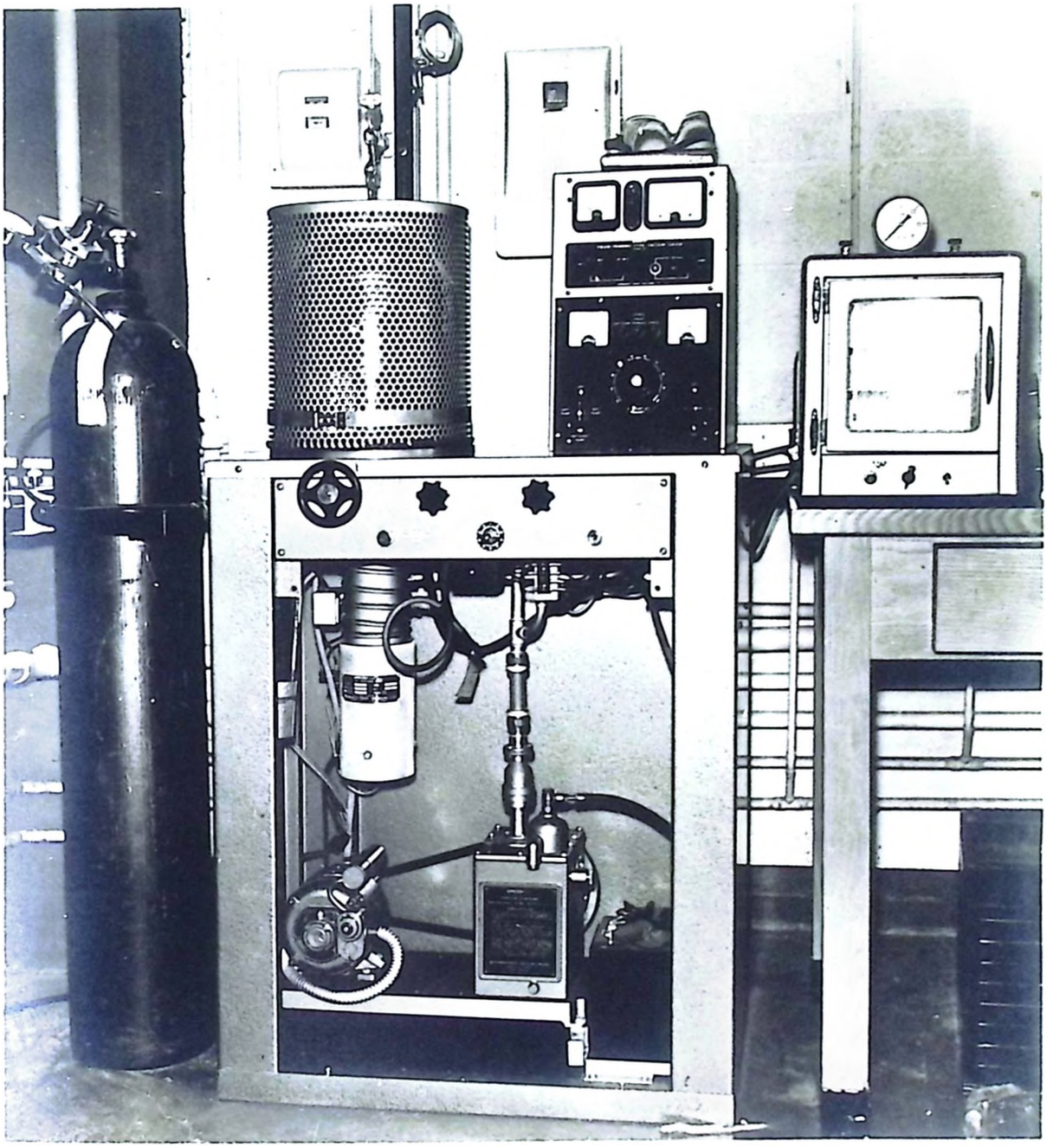

FIGURE 2-1 The "Speedivac" Coating Unit, Model 12E3

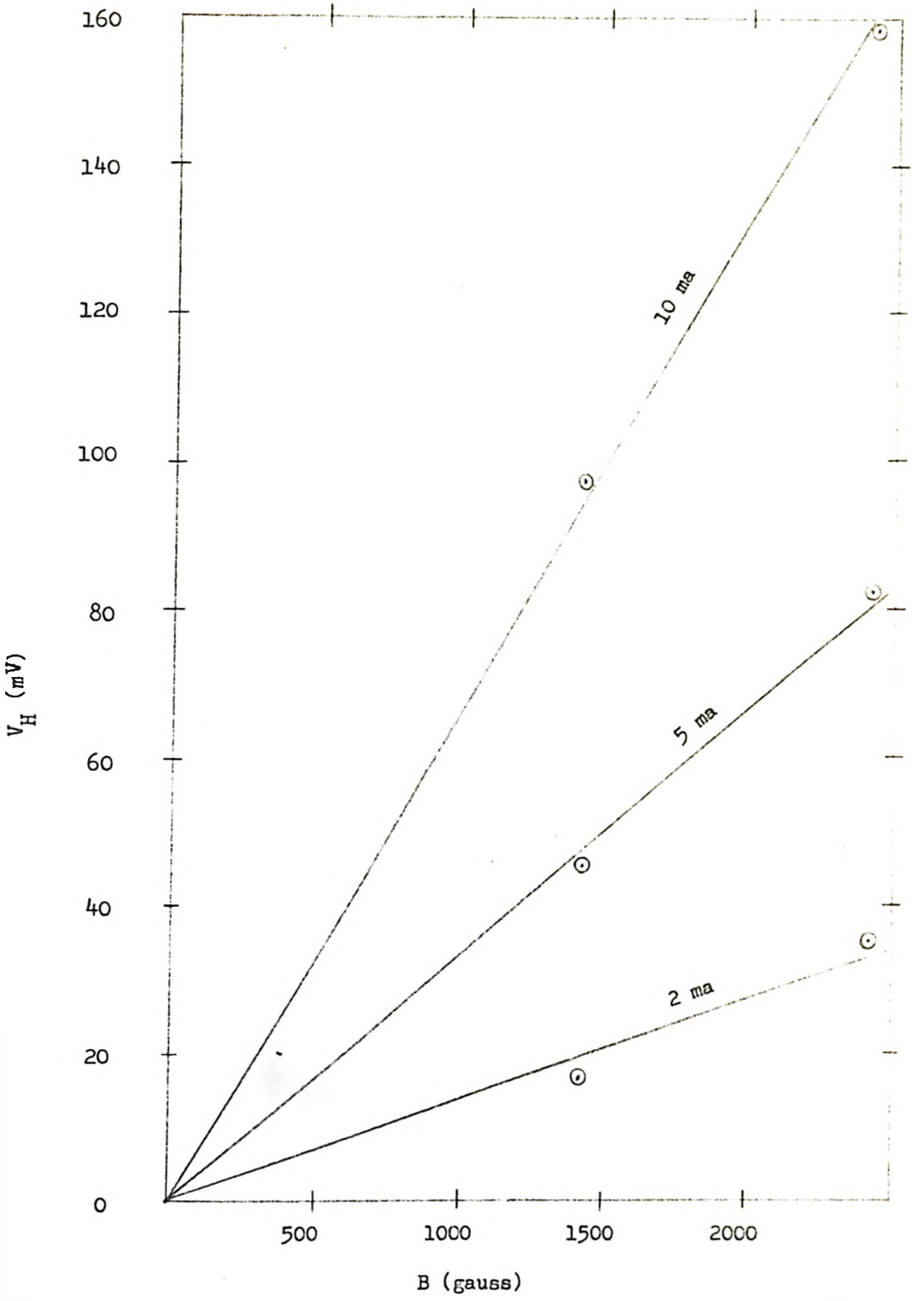

FIGURE 2-2 Hall Voltage vs Magnetic Field

(4800 Å InSb film)

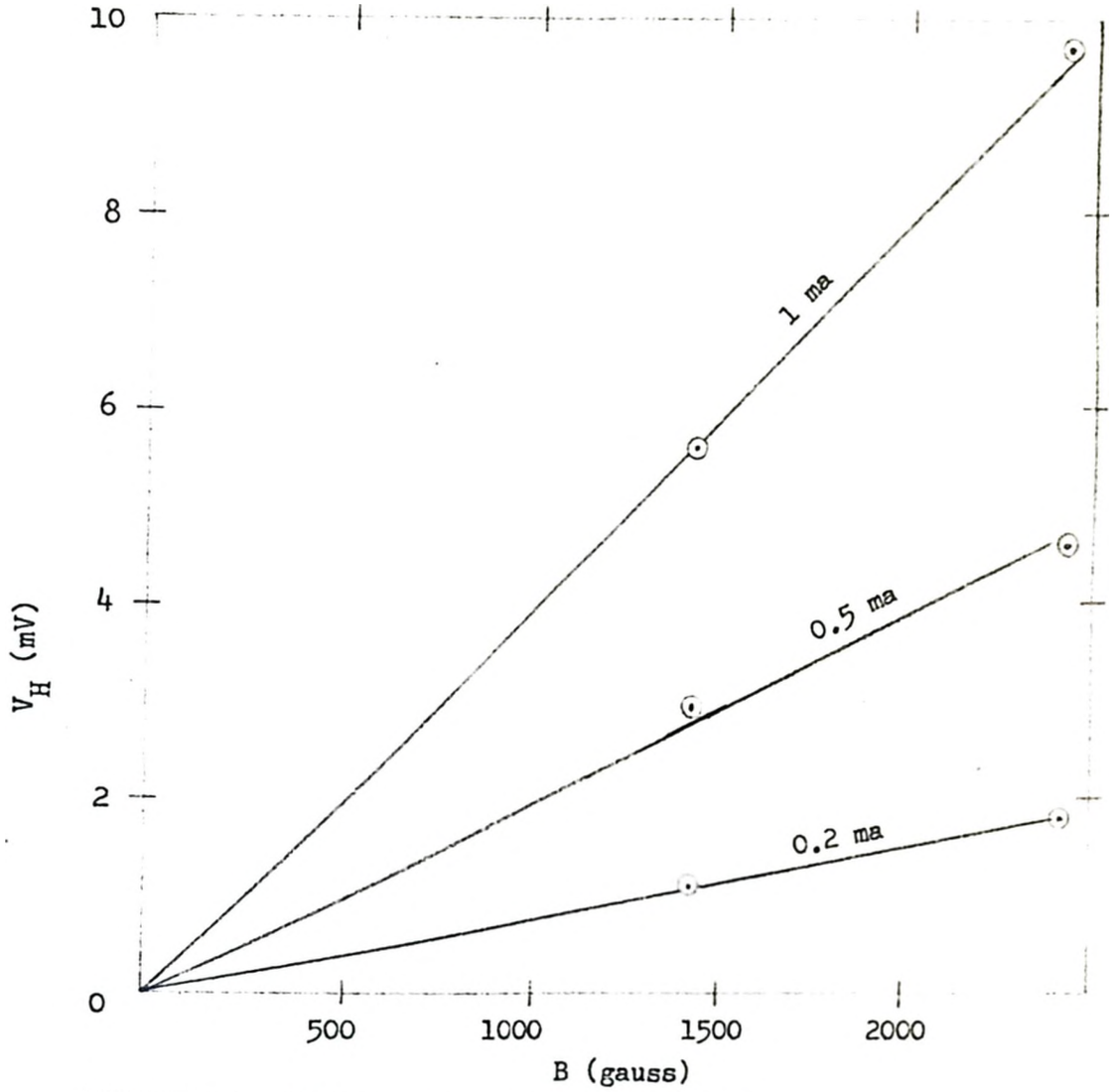

FIGURE 2-3 Hall Voltage vs Magnetic Field
(2180 Å InSb film)

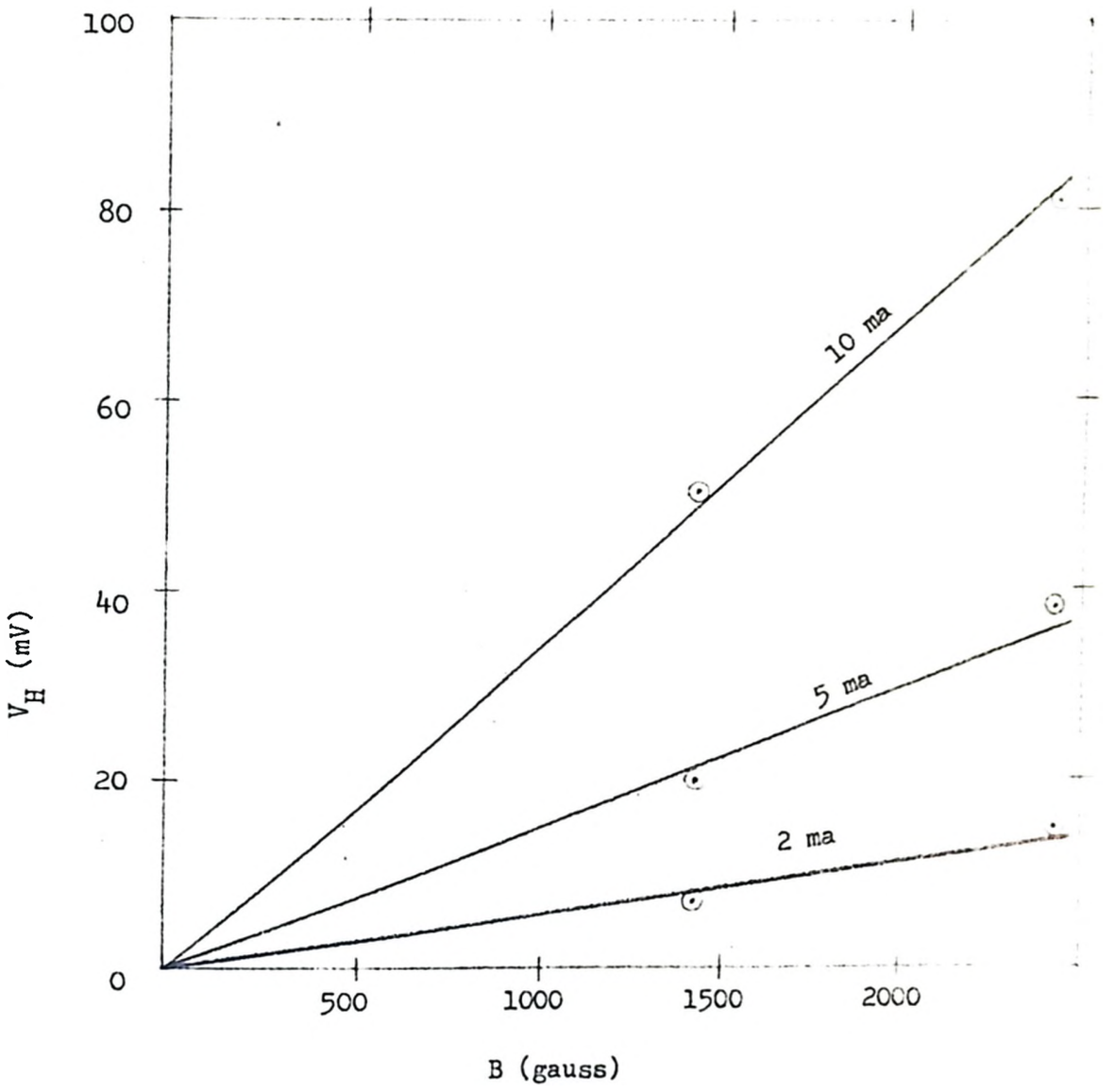

FIGURE 2-4 Hall Voltage vs Magnetic field
(4700 Å InSb film)

Discussion

Present techniques of evaporation do not allow a satisfactory control of the Hall Mobilities of films produced as there is no facility to measure the annealing temperature of the substrate.

For films deposited with the same amount of material per layer and the same annealing temperature, the Hall Mobilities increase almost linearly with thickness, but the resistivities (or conductivities) remain almost the same, in the range between 2000 Å and 5000 Å.

As shown in the results, a film with many layers has a relatively high Hall Mobility compared with a film with fewer layers even though they have the same overall thickness.

To obtain films with higher mobility it appears necessary to employ the technique of simultaneous evaporation of the individual constituents of the material.

CHAPTER III

Microwave Equipment

The system diagram is shown in Figure 3-1 with experimental set up in Figure 3-2 and Figure 3-3.

The different components of the microwave bridge are as follows:

A) Kystrons

2K25 Reflex Klystrons are used as the signal oscillator and the local oscillators. Their characteristics are shown in Table 3-1. For the maximum output power and minimum frequency deviation, the two klystrons are both operated with beam voltage at 300 V at reflector voltage at 160 V.[30]

B) Isolators - Phillips PP4422 ferrite isolators.

For operating range between 8.4 to 9.7 Gc/s the characteristic curves of both the direct and reverse attenuation of the ferrite isolator PP4422X show curves symmetric about 9.0 Gc/s with a maximum of 30 db for the reverse attenuation and a minimum of 0.5 db for the direct attenuation.

C) Attenuators and Phase Shifters (by substitution method)

In this calibration process, the standard attenuator and phase shifter are : -

hp X 382A (series 5945) attenuator.

Accuracy is ± 2% of reading or 0.1 db whichever is greater.

Phase shifter variation is less than 3° from 0 to 50 db.

hp X 885A (series 1094) phase shifter.

Accuracy is 2° (8.2 - 10 Gc) or 3° (10 - 12.4 Gc)

Loss variation 0.3 db max. (8.2 - 10 Gc)

or 0.4 db max. (10 - 12.4 Gc)

All calibration curves of different attenuators and phase shifters are to be found in Figure 3-4 to Figure 3-6.

D) Film-loaded waveguide.

The waveguide was made up of two identical half-sections to allow the film to be mounted between them. The surfaces of the two contacting section which eventually became the longitudinal centre-line of the guide were carefully machined to give a good mechanical fit. The mica sheet on which the film was deposited was thin enough to make any radiation losses negligible.

E) I.F. Amplifier (APS31A).

This I.F. amplifier contained seven stages with a crystal diode in series with 10 KΩ rectifier output stage and has a bandwidth of 6 Mc/s centred at 60 Mc/s. The I.F. amplifier Power supply operates at (a) plate supply 105 V., 60 ma. (b) grid control from zero to 6.5 V. and (c) filament supply 6.3 V. (D.C.), 2.5 amp. The characteristic curves of this I.F. Amplifier are shown in Figure 3-7, Figure 3-8 and Figure 3-9.

Table 3-1

2K25 Reflex Klystron Characteristics[29]

Heater	6.3 V, 0.43 amp (a.c.)
Frequency range	8.5 - 9.66 Gc.
Beam voltage	300 volts.
Beam current	22 ma.
Reflector voltage	110 - 170 volts
Power output	28 mW.
Electronic tuning range	45 Mc.
Electronic tuning rate	2.2 Mc per reflector voltage

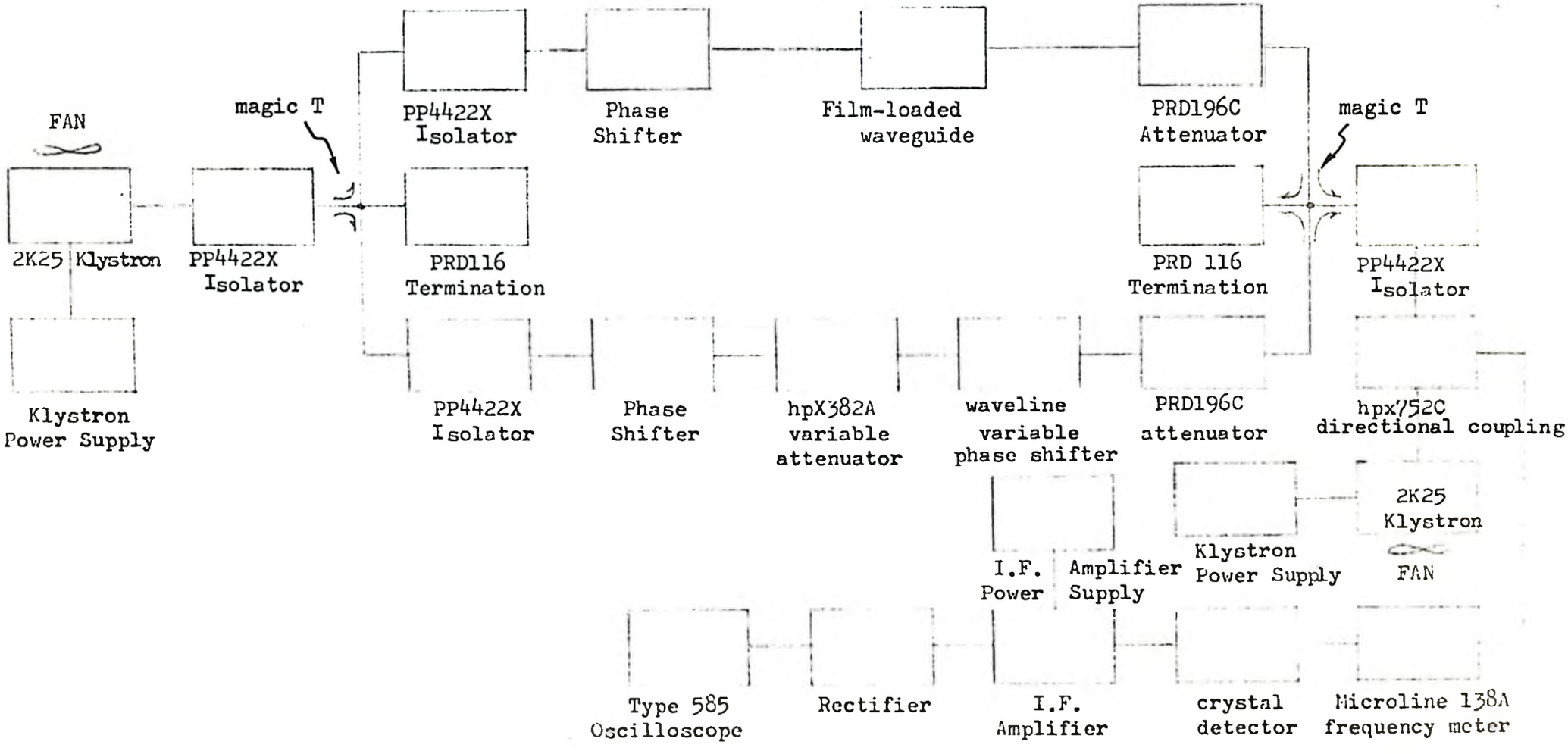

FIGURE 3-1 Microwave Bridge

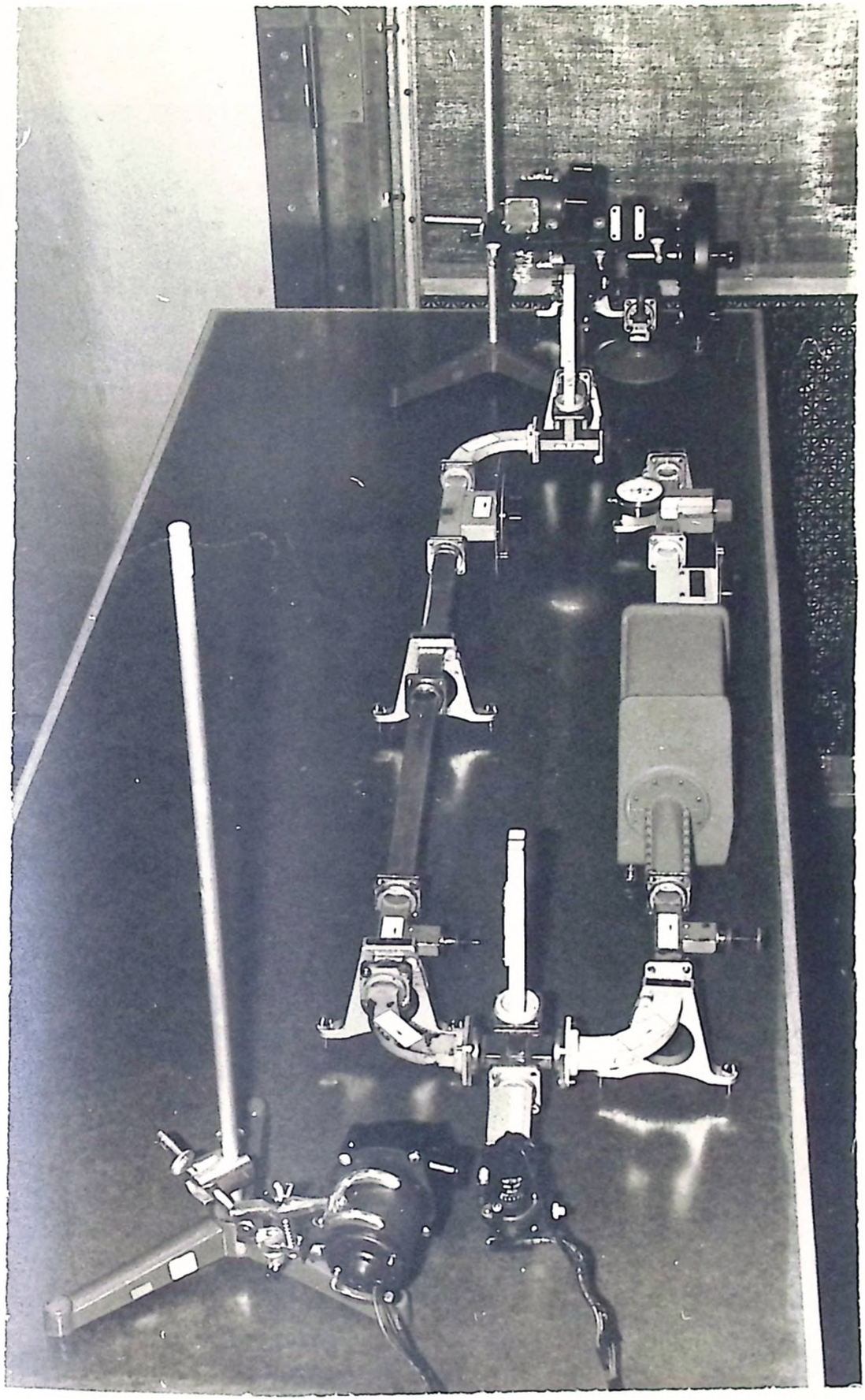

FIGURE 3-2 Experimental set up of Microwave Bridge

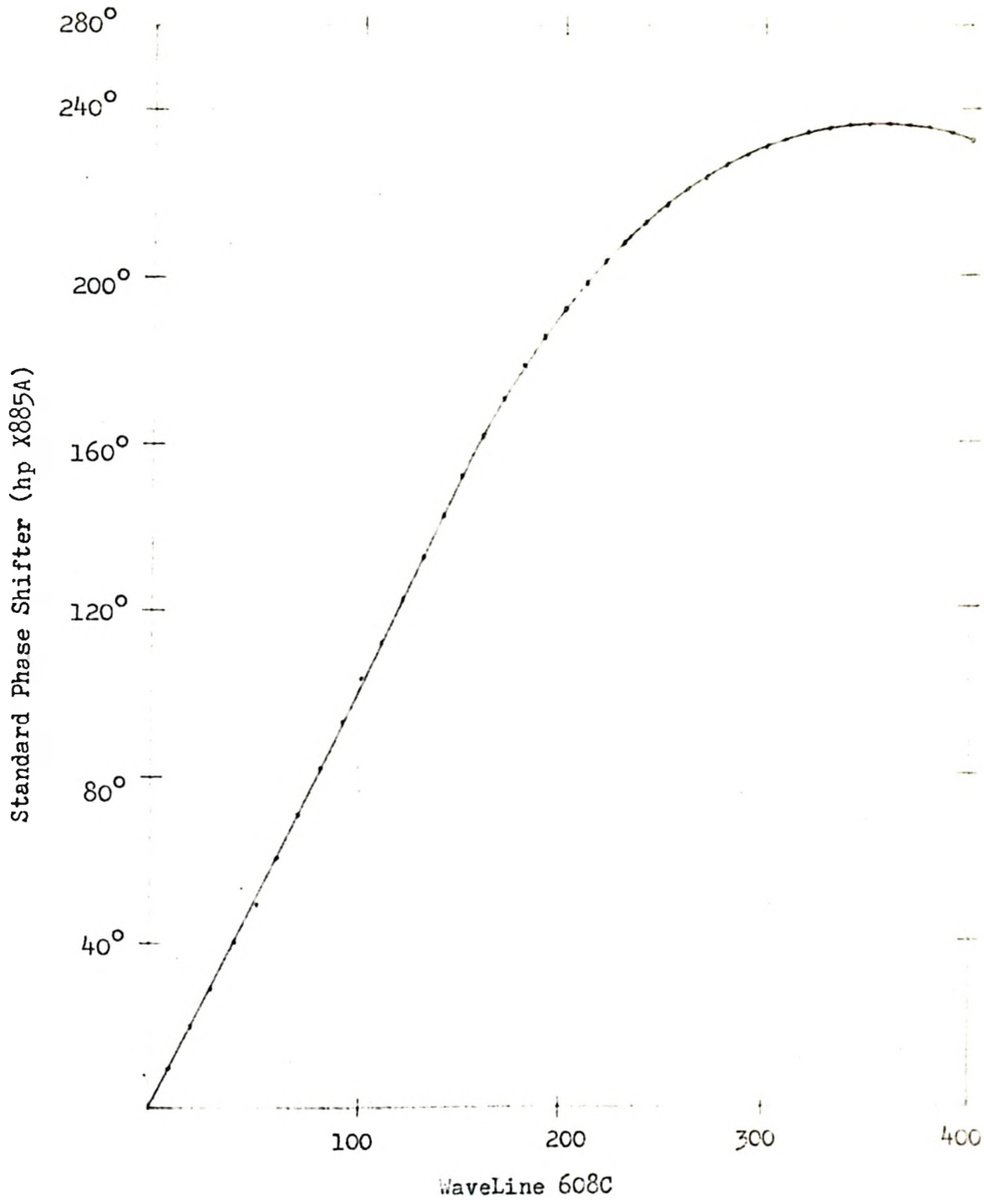

Waveline 608C Phase Shifter Calibration

FIGURE 3-4

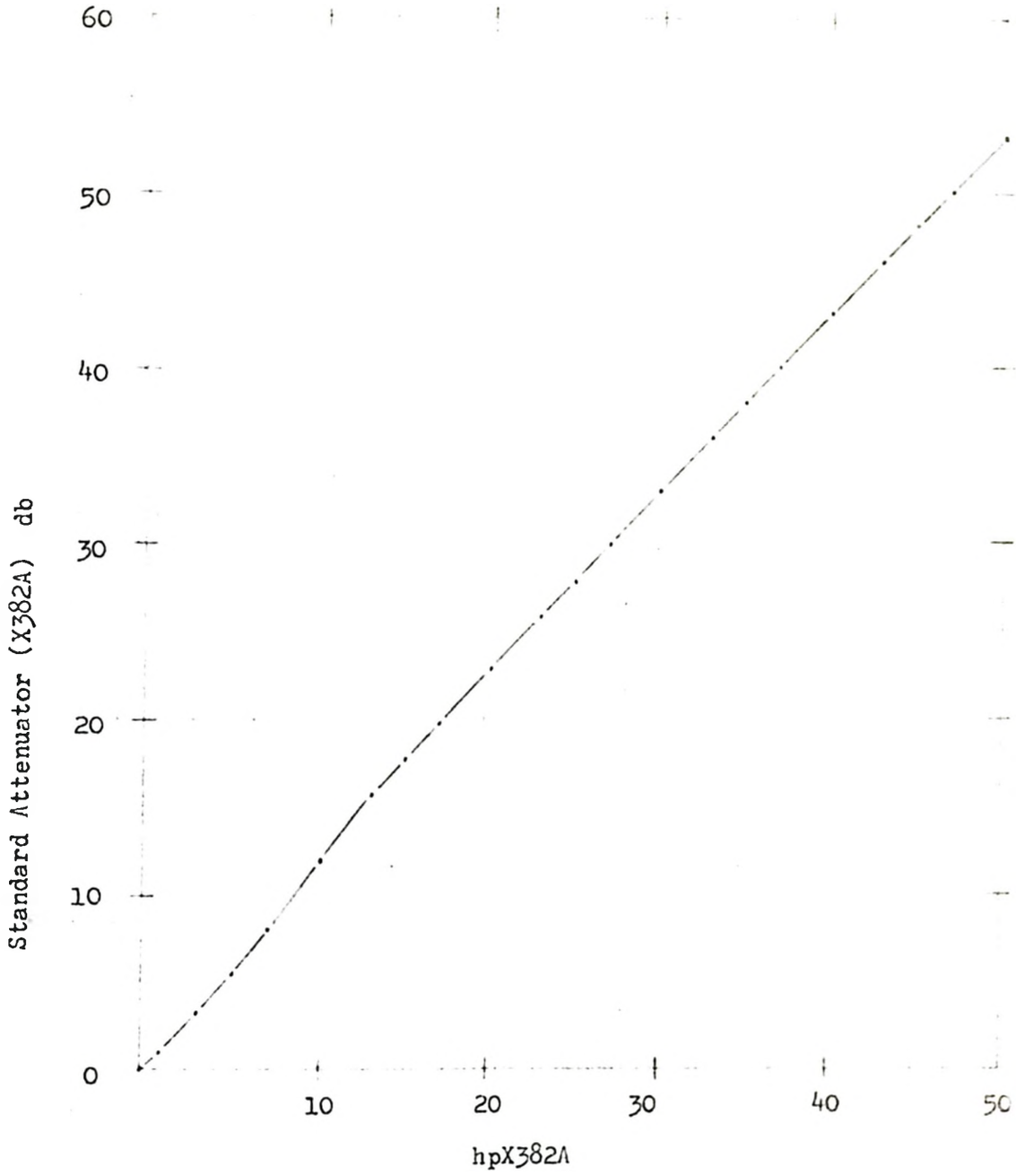

hpX382A Attenuator Calibration

FIGURE 3-5

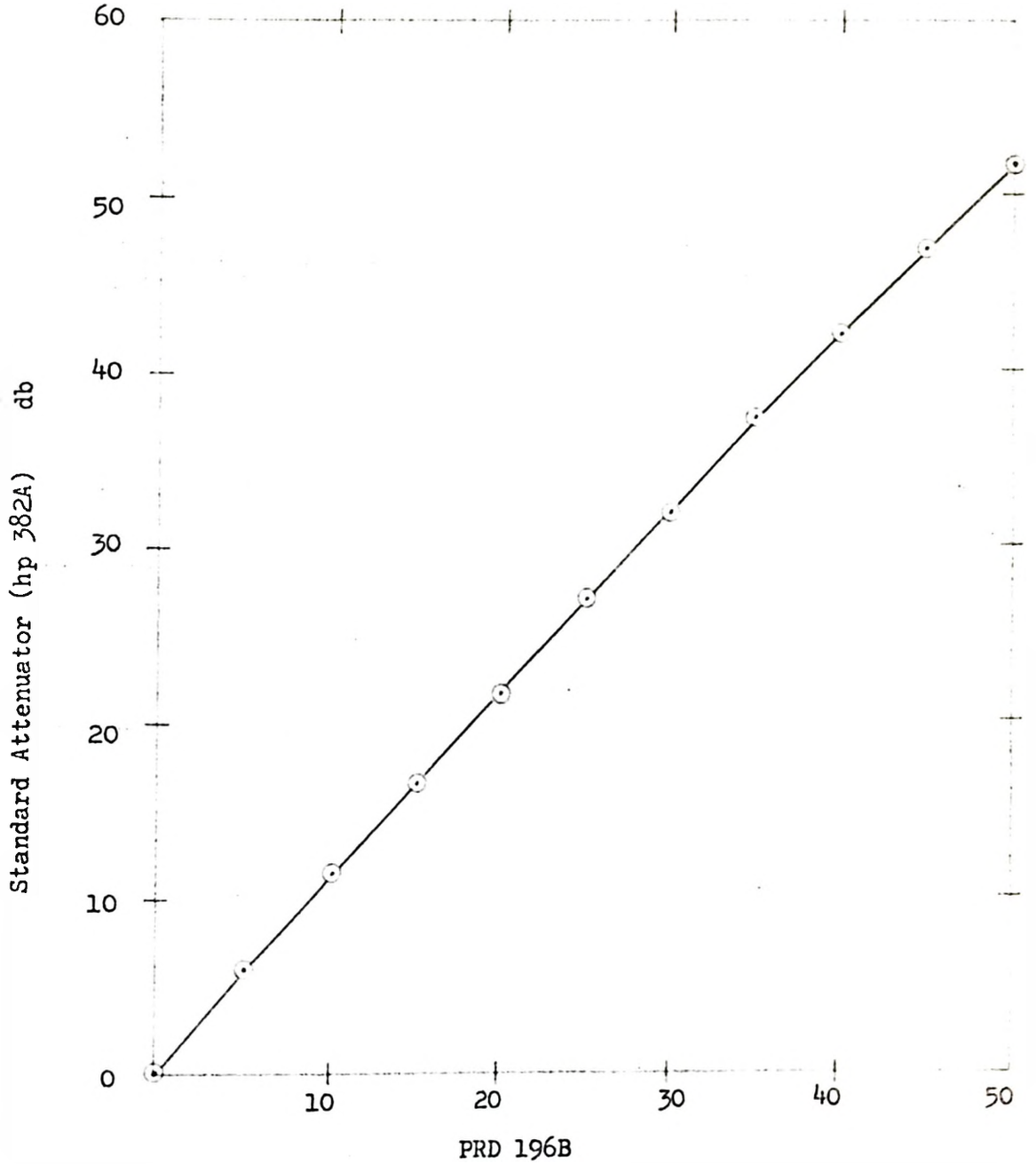

PRD 196B Attenuator Calibration
FIGURE 3-6

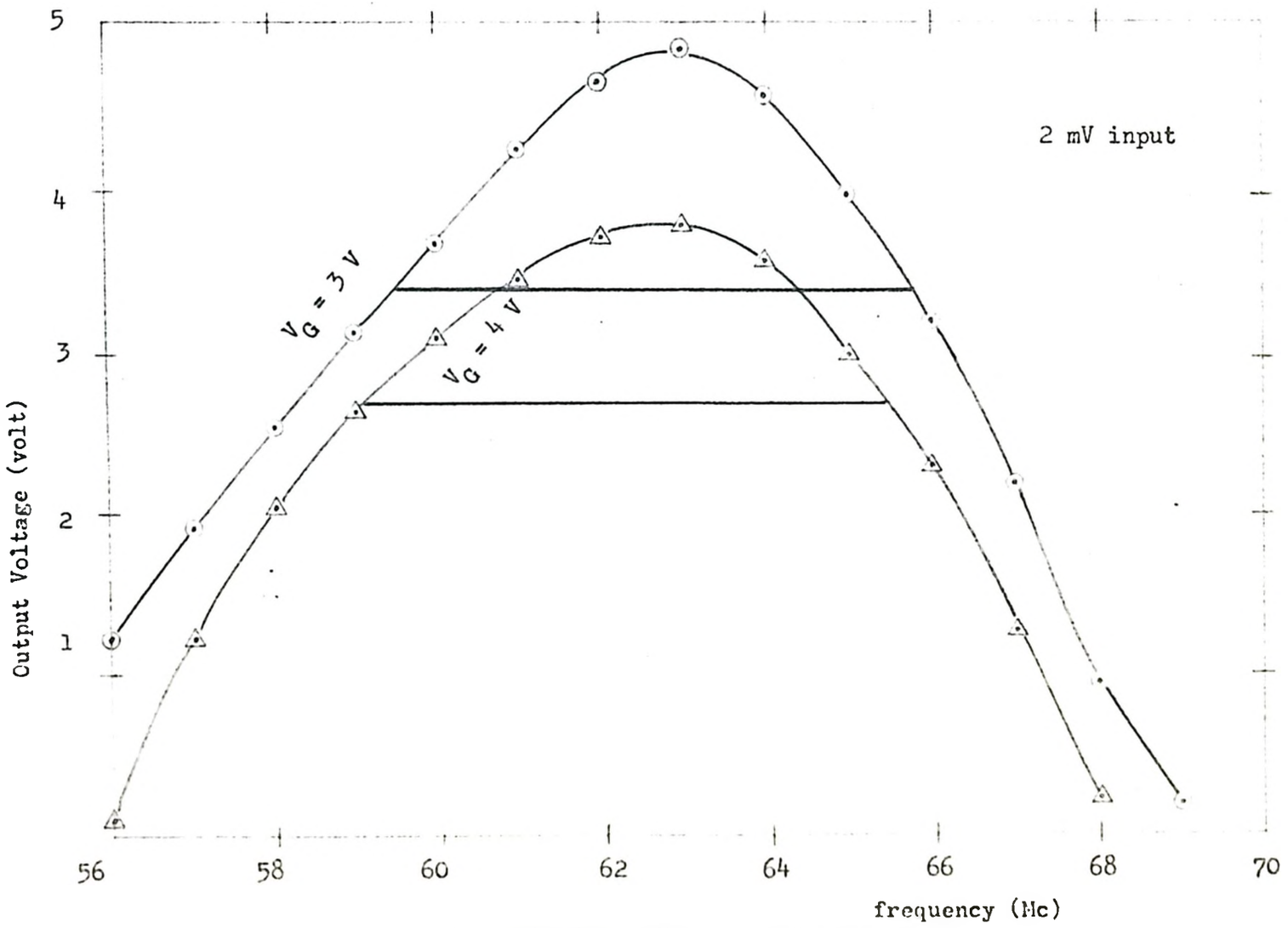

I.F. Amplifier - Frequency Response

FIGURE 3-7

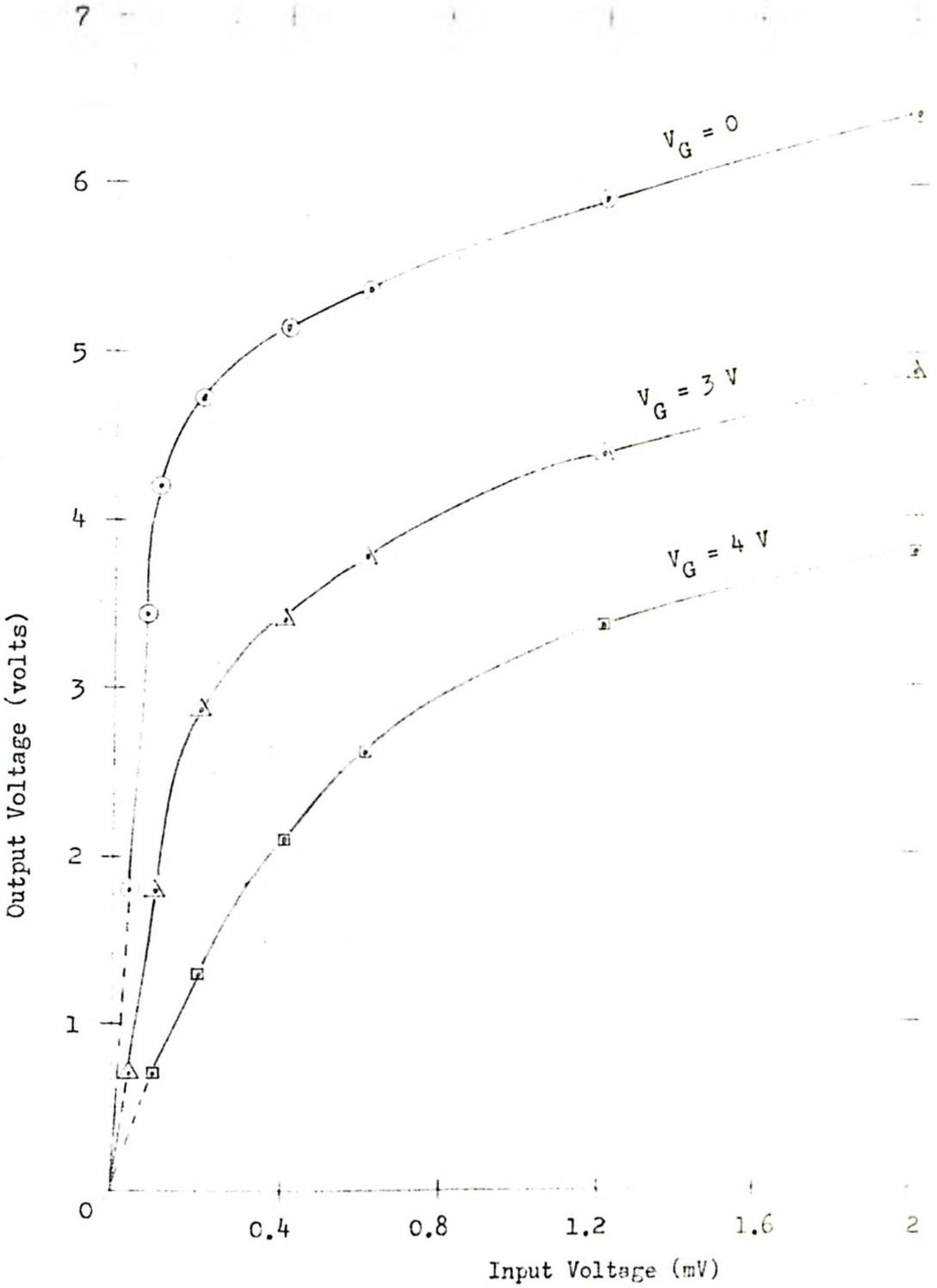

I.F. Amplifier - Output vs Input
FIGURE 3-8

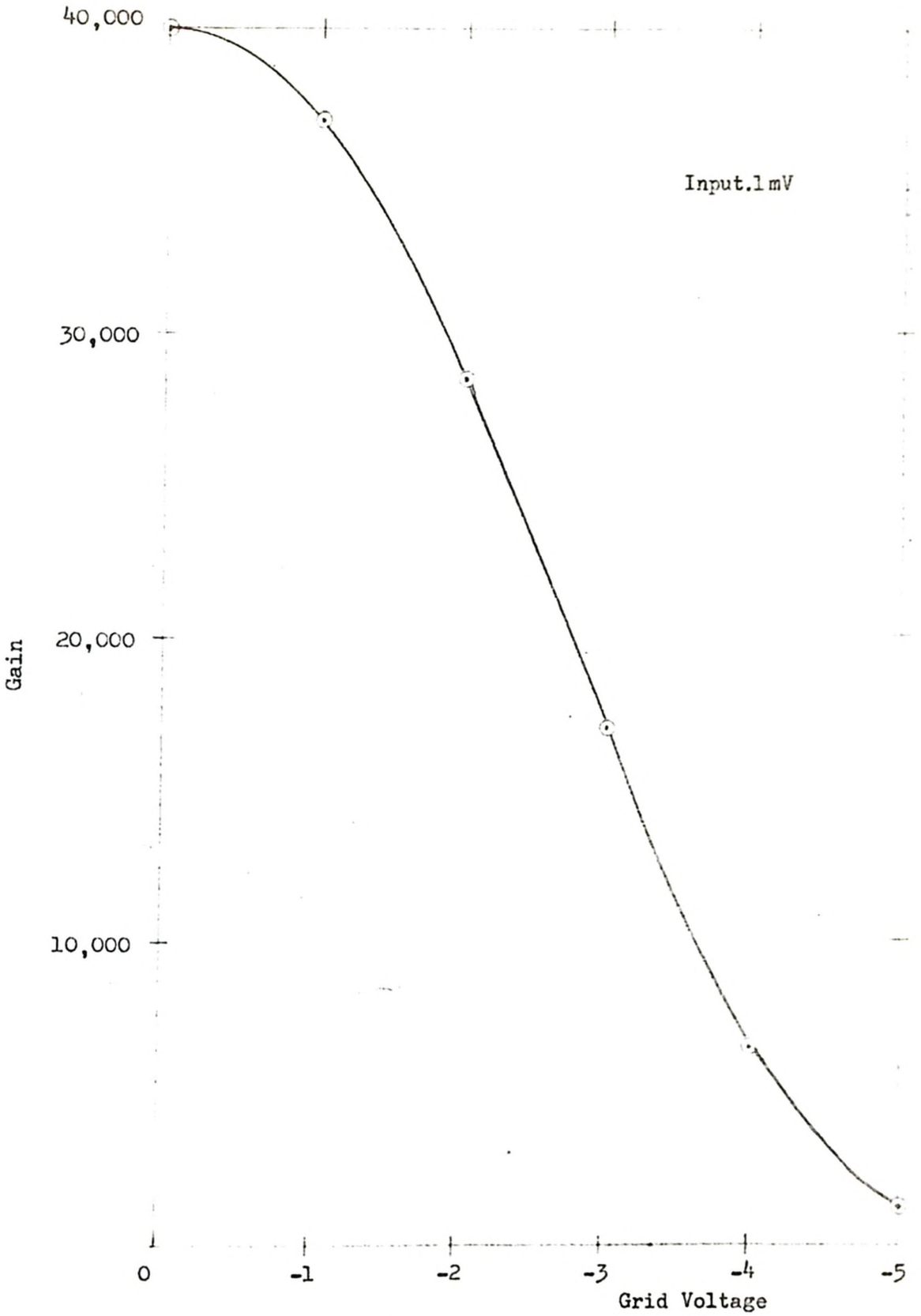

I.F. Amplifier - Gain vs Grid Voltage

FIGURE 3-9

CHAPTER IV

Transmission Characteristics of Film-loaded Waveguide

The normal modes of propagation for guides loaded longitudinally (z-direction) with slabs are not, in general, either T.E. or T.M. modes, but a combination of a T.E. and a T.M. mode.[32][33] If it is a transverse slab, the boundary conditions at the slab-air interface can be satisfied by T.E. (to z direction) modes alone or T.M. (to z direction) modes alone. For a longitudinal slab, the boundary conditions at the slab-air interface is the same as for a transverse slab, except that the slab-air interface is longitudinal rather than transverse. This suggests that the basic modes of propagation for longitudinal slab-loaded rectangular guides are T.E. to X modes or T.M. to X modes if the slab parallel narrow walls of the guide (y-z plane) and T.E. to y modes or T.M. to y modes if the slab parallel broad walls of the guide (x-y plane). Those modes are called Hybrid modes[34] or Longitudinal-Section Electric (LSE) modes and Longitudinal-Section Magnetic (LSM) modes.[32]

Consider a semi-conducting film, the surface of the film being parallel to the narrow walls of a rectangular waveguide and the distance from the narrow wall being "d", as shown in Figure 4-1.

It is assumed that the film has negligible thickness compared with the guide dimension, "a", and makes perfect electrical contact with the two broad walls of the guide. The unloaded waveguide of ratio

b/a = 1/2 is considered to support only modes of the TEmn type[35] so the modes of propagation for the film-loaded rectangular guide are LSE modes (T.E. to x modes). The wave equations

$$\nabla^2\bar{E} = \mu_o\epsilon_o \frac{\partial^2\bar{E}}{\partial t^2} \qquad \nabla^2\bar{H} = \mu_o\epsilon_o \frac{\partial^2\bar{H}}{\partial t^2}$$

here M.K.S. rationalized units are used.

three-dimensional ∇^2 may be broken into two parts:

$$\nabla^2\bar{E} = \nabla_{xy}^2 \bar{E} + \frac{\partial^2\bar{E}}{\partial z^2} \qquad \nabla^2\bar{H} = \nabla_{xy}^2 \bar{H} + \frac{\partial^2\bar{H}}{\partial z^2}$$

The last term is the contribution to ∇^2 from derivatives in the axial direction. The first term is the two-dimensional Laplacian in the transverse plane, representing contributions to ∇^2 from derivatives in this plane. Assuming that the dependence of each field component on z and t is given by a factor $e^{-\gamma z+j\omega t}$, the above wave equations may then be written

$$\nabla_{xy}^2 \bar{E} = -(\gamma^2 + k_o^2)\bar{E} \qquad \nabla_{xy}^2 \bar{H} = -(\gamma^2 + k_o^2)\bar{H}$$

where $\gamma = \alpha + j\beta$ and $k_o = \omega^2\mu_o\epsilon_o$

For Transverse Magnetic Waves

$$E_{z1} = A_1 \sin h_x x \sin (n\pi/b)\, y \cdot e^{-\gamma z} \quad \text{for } 0 \leq x \leq d$$

$$E_{z2} = A_2 \sin h_x(a-x) \sin (n\pi/b)\, y \cdot e^{-\gamma z} \quad \text{for } d \leq x \leq a$$

as derived in Appendix D.

Similarly for Transverse Electric Waves

$$H_{z1} = B_1 \cos h_x x \cos (n\pi/b)\, y \cdot e^{-\gamma z} \quad \text{for } 0 \leq x \leq d$$

$$H_{z2} = B_2 \cos h_x (a-x) \cos (n\pi/b)\, y \cdot e^{-\gamma z} \quad \text{for } d \leq x \leq a$$

The field components for LSE modes derived in Appendix E are:

for $0 \leq x \leq d$

$$E_{x1} = 0$$

$$E_{y1} = - \frac{\gamma}{(n\pi/b)} A \sin h_x x \cos (n\pi/b)\, y \cdot e^{-\gamma z}$$

$$E_{z1} = A \sin h_x x \sin (n\pi/b)\, y \cdot e^{-\gamma z}$$

$$H_{x1} = \frac{j(k_o^2 - h_x^2)}{\omega\mu_o (n\pi/b)} A \sin h_x x \cos (n\pi/b)\, y \cdot e^{-\gamma z}$$

$$H_{y1} = \frac{jh_x}{\omega\mu_o} A \cos h_x x \sin (n\pi/b)\, y \cdot e^{-\gamma z}$$

$$H_{z1} = \frac{j\gamma h_x}{\omega\mu_o (n\pi/b)} A \cos h_x x \cos (n\pi/b)\, y \cdot e^{-\gamma z}$$

for $d \leq x \leq a$

$$E_{x2} = 0$$

$$E_{y2} = - \frac{\gamma}{h_y} B \sin h_x (a-x) \cos (n\pi/b)\, y \cdot e^{-\gamma z}$$

$$E_{z2} = B \sin h_x (a-x) \sin (n\pi/b)\, y \cdot e^{-\gamma z}$$

$$H_{x2} = \frac{j(k_o^2 - h_x^2)}{\omega\mu_o (n\pi/b)} B \sin h_x (a-x) \cos (n\pi/b)\, y \cdot e^{-\gamma z}$$

$$H_{y2} = - \frac{jh_x}{\omega\mu_o} B \cos h_x (a-x) \sin (n\pi/b)\, y \cdot e^{-\gamma z}$$

$$H_{z2} = \frac{j\gamma h_x}{\omega\mu_o (n\pi/b)} B \cos h_x (a-x) \cos (n\pi/b)\, y \cdot e^{-\gamma z}$$

The above equations satisfy the boundary conditions at the surface of the waveguide, but in addition the boundary conditions at the surface of the film have to be complied with:

$$E_{y1} = E_{y2} = E_y \quad \text{at} \quad x = d$$

which gives $B = \dfrac{\sin h_x d}{\sin h_x(a-d)} A$ from above equations.

If Y is the admittance of the film per square, the maxwell curl equation for the magnetic field $\nabla \times H = J$ or $\oint H.d\ell = I$

which gives $H_{z1} - H_{z2} = \dfrac{I}{\ell} = E_y Y$ at $x = d$.

$$\therefore \frac{j\sigma h x}{\omega\mu_o(m\pi/b)} \left[A \cos h_x d + B \cos h_x(a-d)\right] = Y \frac{Y}{(m\pi/b)} A \sin h_x d$$

In substituting for B in terms of A and rearranging, the following characteristic equation is obtained

$$h_x \left[\cot h_x d + \cot h_x(a-d)\right] = -j\omega\mu_o Y$$

If $Y = G + jB$, the characteristic equation becomes,

$$\frac{u \sinh (2dv/a) - v \sin (2du/a)}{\cosh (2dv/a) - \cos (2du/a)} + \frac{u \sinh 2(a-d)v/a - v \sin 2(a-d)u/a}{\cosh 2(a-d)v/a - \cos 2(a-d)u/a} = \omega\mu_o aG$$

$$\frac{u \sin (2du/a) + v \sinh (2dv/a)}{\cosh (2dv/a) - \cos (2du/a)} + \frac{u \sin 2(a-d)u/a + v \sinh 2(a-d)v/a}{\cosh 2(a-d)v/a - \cos 2(a-d)u/a} = \omega\mu_o aB$$

where $G = \sigma t_f$ or $1/R$ is the conductance of the film per square and $B = (\omega\varepsilon_r\varepsilon_o) t_f$ [35] is the susceptance of the film per square. (σ is the conductivity of the film per square, t_f is the thickness of the film and

ε_r is the relative permittivity of the film, for indium antimonide $\varepsilon_r = 16$). Now consider the wavelength range in which only the dominant mode can propagate in the unloaded guide; i.e. n = 0 and the film is located at the center of the waveguide, i.e. $d = \frac{a}{2}$. The characteristic equations are simplified to

$$\frac{u \sinh v - v \sin u}{\cosh v - \cos u} = \frac{\omega\mu_o aG}{2}$$

$$\frac{u \sin u + v \sinh v}{\cosh v - \cos u} = \frac{\omega\mu_o aB}{2}$$

the attenuation coefficient, α, and the phase-change coefficient, β, can be obtained from the equation relating the wave numbers for each direction taking $h_y = 0$ (see Appendix D)

$$\gamma^2 = h_x^2 - k_o^2$$

$$= \left(\frac{u + jv}{a}\right)^2 - \omega^2\mu_o\varepsilon_o$$

$$= \left(\frac{u^2 - v^2}{a^2}\right) - \omega^2\mu_o\varepsilon_o + j\frac{2uv}{a}$$

$$(\alpha+j\beta)^2 = \text{Re} + j\text{Im}$$

$$= \sqrt{(\text{Re})^2 + (\text{Im})^2}\; e^{-j\theta}$$

$$\text{where } \theta = \tan^{-1}\left(\frac{\text{Im}}{\text{Re}}\right)$$

$$\alpha + j\beta = \left[(Re)^2 + (Im)^2\right]^{1/4} e^{j\frac{\theta}{2}}$$

$$\alpha = \left[(Re)^2 + (Im)^2\right]^{1/4} \cos\frac{\theta}{2}$$

$$\beta = \left[(Re)^2 + (Im)^2\right]^{1/4} \sin\frac{\theta}{2}$$

The solution of α and β can be obtained numerically when the admittance of film, Y, and the position of insertion, d, are given. The IBM 7040 computer program II is the numerical calculation for the propagation coefficient, γ, with different admittances of the film, Y, $R = \frac{1}{G}$ from 50 ohm per square to 50 MΩ per square, $B = 10^{-6}$ 1/Ω per square and f, frequency, is 9.25 Gc/s. The results are shown in Figure 4-2.

Theoretical Results

Propagation Constant of InSb film-loaded waveguide

Frequency = 9.25 Gc/s Relative Permittivity = 16

Resistance per square R(Ω)	Phase-change Coefficient β(rad/m)	Attenuation Coefficient α(N/m)
0.0	0.00026136	194.88239
0.5 x 10	4.64540690	194.85430
1.1 x 10	10.23248899	194.74502
1.7 x 10	15.84847641	194.54823
2 x 10	18.67211700	194.41422
5 x 10	47.86961651	191.22701
1 x x 10^2	97.04055309	169.60545
2 x 10^2	131.08980942	106.11738
5 x 10^2	136.62243271	45.85230
1 x 10^3	136.78953361	23.25631
2 x 10^3	136.79005241	11.67270
5 x 10^3	136.78686905	4.67418
1 x 10^4	136.78629494	2.33745
5 x 10^4	136.78609657	0.46751
1 x 10^5	136.78609657	0.23376
5 x 10^5	136.78635025	0.04675
1 x 10^6	136.78609848	0.02338
5 x 10^7	136.78609657	0.00467
1 x 10^8	136.78609276	0.00233
5 x 10^8	136.78609467	0.00046

Experimental Results

Attenuation and Phase Shift of InSb films and micas

Sample	Film I	Film II	Film III	Film IV	mica I	mica II
Resistance per square	1375Ω	926Ω	846Ω	414Ω	-	-
dimension	3.6cm X 2.75cm	3.6cm X 2.7cm	3.6cm X 2.7cm	4.7cm X 2.95cm	3.6cm X 2.7cm	4.7cm X 2.95cm
Attenuation	5.50 db 5.40 5.55 5.60 5.60	8.20 db 8.10 8.20 8.05 8.15	8.65 db 9.05 8.9 8.85 9.05	23.0 db 24.5 24.0 20.0 23.0	0.35 db 0.35 0.40 0.35	0.2 0.2 0.2 0.15 0.175
average attenuation	5.53 db	8.14 db	8.96 db	23.625 db	0.35 db	0.2 db
attenuation coefficient	0.166 N/cm	0.25 N/cm	0.276 N/cm	0.43 N/cm		
Phase Shift	7.0° 5.0° 6.5° 5.5° 6.0°	7° 10.5° 6.5° 7.0° 8.0°	7.5° 6.5° 9.0° 7.0° 8.5	9.5° 9.0° 9.0° 9.0° 9.0°	5.5° 6.0° 5.5 4.0	6.0 6.5 5.5 6.0 6.0
Average Phase Shift	6.0°	7.125°	7.7°	9.0°	5.7°	6.0°
Phase Change Coefficient	0.0290 rad/cm	0.0345 rad/cm	0.0373 rad/cm	0.0334 rad/cm	-	-
empty guide Phase change coefficient (f=9.25 gc/s)	1.3675 rad/cm	1.3675 rad/cm	1.3675 rad/cm	1.3675 rad/cm	-	-
film-loaded wave-guide Phase Change coefficient	1.3965 rad/cm	1.402 rad/cm	1.4048 rad/cm	1.4009 rad/cm	-	-

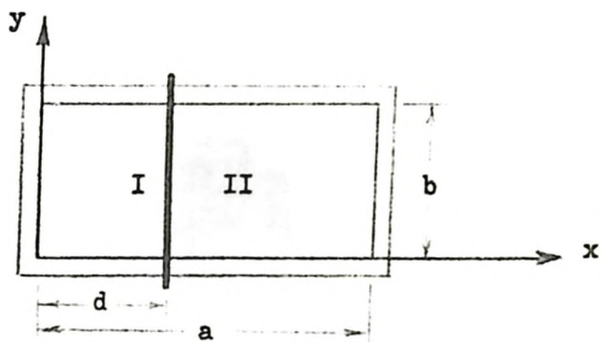

FIGURE 4-1

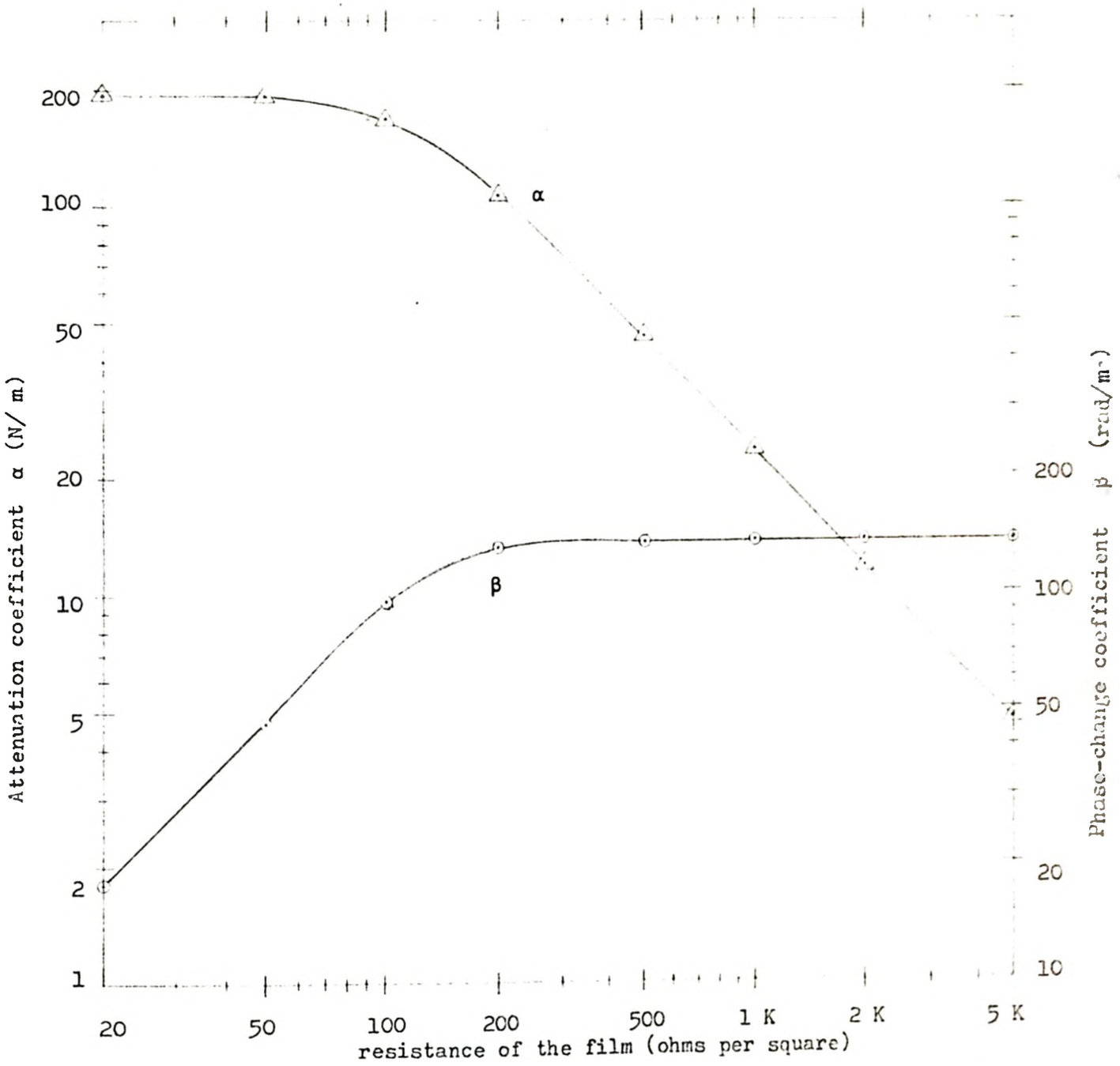

FIGURE 4-2 Propagation Coefficient of film-loaded waveguide

Discussion

The second computer 7040 programme "Propagation Coefficient of film-loaded waveguide" is to analyze at different microwave frequencies the complex phase-change coefficient in the direction of propagation in a rectangular waveguide with a thin film located at the centre of the guide with the surface of the film parallel to the narrow wall of the guide. The complex phase-change coefficients are given in both rectangular form ($\gamma = \alpha + j\beta$) and polar form ($\gamma = |\gamma| e^{i\theta}$) for different impedance of the film. The complex numbers in the direction perpendicular to the surface of the film can also be obtained from this programme.

Four In-Sb films with different resistances per square (1375Ω, 926Ω, 846Ω and 414Ω) have been measured. Their measured values of attenuation and phase shift are found to be very close to the theoretical values in Figure 4-2.

CONCLUSIONS

A sensitive microwave bridge and a high voltage pulse generator have been assembled for the measurements of the changes in the complex permittivities of indium antimonide thin films subjected to high electric fields. The bridge, operating at a frequency of 9.25 Gc/s, is capable of measuring attenuations and phase shifts of waveguide sections with a loss of 40 db to an accuracy approaching 0.1 db and 1.0 degree respectively. An I.F. amplifier with a bandwidth of 6 Mc/s, centred at 60 Mc/s, and a gain of 80 db is used to detect the output of the microwave bridge. It is found that the output of the Klystron 2K25 is temperature dependent due to thermal expansion of the resonant cavity. Consequently a blower has been used for cooling to maintain constant temperature.

A new type of high voltage pulse generator has been designed. This features a continuously variable pulse width from 0.2 μ sec. to 5 μ sec. with a low output impedance of approximately 13 ohms and a repetition rate adjustable to 1, 2, 5 and 10 pulses per sec. The theoretical model of the pulse generator (Figure 1-6) and the theoretical solution for the rise time of the output pulse derived thereof (Appendix B) are shown to be valid as seen in the 4 Kv, 0.5 μ sec. pulse measurements (Figure 1-15). These measurements have shown that during conduction the equivalent circuit of the thyratron type 5C22 consists of a major capacitance (grid-anode) of 15 pf., and inductance (anode- cathode) of 2 μh and a resistance of 2.36

Films of indium antimonide with thickness of the order of 10^3 Å have been prepared by vacuum deposition onto thin mica substrates. To obtain high Hall mobilities, a multilayer construction with subsequent annealing has been used. The Hall mobilities obtained ranged between 500 and 1000 $cm^2/V\text{-}sec$.

It has been found that a linear relationship exists between the Hall mobility and the film thickness in the range between 2000 Å and 5000 Å, but that the conductivities remain almost constant. For the same film thickness the Hall mobility increases with number of layers. The annealing temperature has a large influence on the mobilities of the film. A study into this effect would have extended the range of mobilities, but due to lack of facilities at the present time, this has not been done. Temperatures inside the vacuum coating unit would be measured with a chromo-nickel thermocouple connected through a "covar seal" and also provision of independent heater boats for the evaporation of the indium and antimony separately would be desirable.

A theoretical solution of the complex propagation constant of a film-loaded waveguide is presented. The film is placed longitudinally in a rectangular waveguide with the surface of the film parallel to the narrow wall of the guide in a fashion similar to the ordinary vane-type attenuator. This solution is calculated numerically with an IBM 7040 computer programme (Appendix F) by Newton's method of iteration. The complex propagation constants are given in both rectangular form ($\gamma = \alpha + j\beta$) and polar form ($\gamma = |\gamma| e^{j\theta}$) for different values of the film impedance. The complex wave numbers in the direction perpendicular to the surface of

the film for different impedance of the film can be also obtained from this computer programme.

The propagation constant of film-loaded waveguide for a film located at the centre of the guide with the surface of the film parallel to the narrow wall of the guide has been solved with the computer programme. This programme is also applicable to films located longitudinally with the surface parallel to the broad wall of the guide if the field components for T.E.mn to y modes were used instead of T.E.mn to x modes as discussed in Appendix E. Various distances between the film and the waveguide wall can also be calculated. Furthermore, not only the dominant mode propagates in the unloaded guide, but also the study of the other modes can be obtained by changing the transverse wave numbers, e.g. for TE_{11} mode $h_y = \frac{\pi}{b}$ or n = 1, instead of n = 0 for the dominant mode TE_{10}.

APPENDIX A

$$I(s) = \frac{V/s}{R_L + Z \coth \delta s}$$

$$= \frac{V/s}{R_L + \frac{Z(e^{\delta s} + e^{-\delta s})}{(e^{\delta s} - e^{-\delta s})}}$$

$$= \frac{V}{s} \times \frac{1 - e^{-2\delta s}}{Z + R_L + (Z - R_L)\, e^{-2\delta s}}$$

$$= \frac{V(1 - e^{-2\delta s})}{s(Z + R_L)} \times \frac{1}{1 + \frac{Z - R_L}{Z + R_L} e^{-2\delta s}}$$

Since $(Z - R_L)^2 < (Z + R_L)^2$ and $e^{-2\delta s} < 1$

or $\left| \frac{Z - R_L}{Z + R_L} e^{-2\delta s} \right| < 1$

$$I(s) = \frac{V(1 - e^{-2\delta s})}{s(Z + R_L)} \left[1 - \frac{Z - R_L}{Z + R_L} e^{-2\delta s} + \left(\frac{Z - R_L}{Z + R_L} \right)^2 e^{-4\delta s} - \cdots \right]$$

APPENDIX B

At $t = 0$ the switch T_1 is closed. The circuit in Figure 1-7 can be represented by Figure B-1 for $0 \geq t \gg t_1$

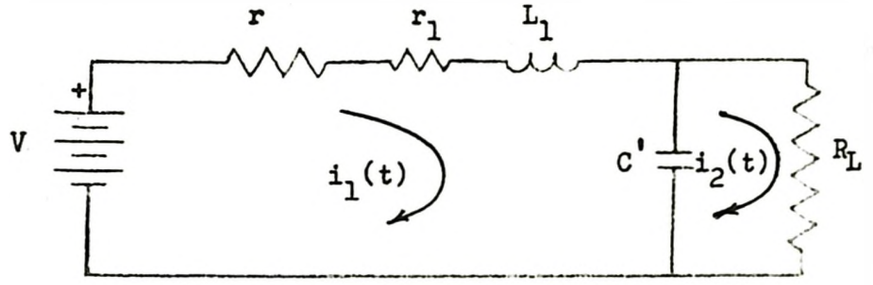

FIGURE B-1

The transform equation of the output current, $I_2(s)$, of this equivalent circuit is found by the determinant

$$I_2(s) = \frac{\begin{vmatrix} r + r_1 + L_1 s + \frac{1}{c's} & \frac{V}{s} \\ -\frac{1}{c's} & 0 \end{vmatrix}}{\begin{vmatrix} r + r_1 + L_1 s + \frac{1}{c's} & -\frac{1}{c's} \\ -\frac{1}{c's} & \frac{1}{c's} + R_L \end{vmatrix}}$$

$$= \frac{V}{L_1 C' R_L s \left[s^2 + s\left(\frac{r + r_1}{L_1} + R_L \frac{1}{C'} \right) + \frac{r + r_1 + R_L}{L_1 C' R_L} \right]}$$

$$= \frac{V}{L_1 C' R_L} \times \frac{1}{s(s - s_1)(s - s_2)}$$

where s_1 and s_2 are the roots of the quadratic equation in the denominator and

$$s_1, s_2 = -\left(\frac{r + r_1}{2L_1} + \frac{1}{2R_L C'}\right) \pm \sqrt{\left(\frac{r + r_1}{2L_1} + \frac{1}{2R_L C'}\right)^2 - \frac{r + r_1 + R_L}{L_1 C' R_L}}$$

$$= -\alpha \pm j\beta$$

$$\text{where } \alpha = \frac{r + r_1}{2L_1} + \frac{1}{2R_L C'}$$

$$\beta = \sqrt{\frac{r + r_1 + R_L}{L_1 C' R_L} - \alpha^2}$$

By use of the method of residues,

$$i_1(t) = \frac{V}{L_1 C' R_L}\left\{\frac{1}{s_1 s_2} + \frac{e^{s_1 t}}{s_1(s_1 - s_2)} + \frac{e^{s_2 t}}{s_2(s_2 - s_1)}\right\}$$

$$= \frac{V}{r + r_1 + R_L}\left\{1 + \frac{s_2 e^{s_1 t} - s_1 e^{s_2 t}}{s_1 - s_2}\right\}$$

Substitute $s_1 = -\alpha + j\beta$ and $s_2 = -\alpha - j\beta$

$$i_2(t) = \frac{V}{r + r_1 + R_L}\left\{1 - e^{-\alpha t}\left(\frac{\alpha}{\beta}\sin \beta t + \cos \beta t\right)\right\}$$

and the output voltage across R_L is

$$V(t) = \frac{VR_L}{r + r_1 + R_L}\left\{1 - e^{-\alpha t}\left(\frac{\alpha}{\beta}\sin \beta t + \cos \beta t\right)\right\}$$

APPENDIX C

IBM 7040 Computer Programme I
for equation (A) in Chapter I.

$$V(t) = \frac{VR_L}{r + r_1 + R_L}\left[1 - e^{-\alpha t}\left(\frac{\alpha}{\beta}\sin\beta t + \cos\beta t\right)\right]$$

```
$JOB              003501 CHAN T.          020    005
$IBJOB            NODECK
$IBFTC
C       PULSER CIRCUIT
        DIMENSION V(25, 5, 5),    T(50),       C(10),RL(10)
        DIMENSION ALPHA(    10,10),BETA(    10,10)
        READ 1, VV,R,RI
        READ 2,(RL(L), L=1,3)
        READ 3, (C(K), K=1,3)
        READ 4, A
        DO 100 L=1,3
        DO 100 K=1,3
        DO 100 I=1,21
        T(I)=(5.*(10.**(-8)))*FLOAT(I-1)
        ALPHA(   K,L)=(R+RI)/(2.*A   )+1./(2.*RL(L)*C(K))
        BETA(   K,L)=SQRT(ABS((R+RI+RL(L))/(A    *C(K)*RL(L))-
       1ALPHA(   K,L)**2))
        V(I,   K,L)=(VV*RL(L)/(R+RI+RL(L)))*(1.-(EXP(-ALPHA(   K,L)*T(I)))*
       1((ALPHA(   K,L)*(SIN(BETA(   K,L)*T(I))))/BETA(   K,L)+
       1COS(BETA(   K,L)*T(I))))
  100 PRINT 222, (T(I),V(I,   K,L))
  222 FORMAT (20X,E10.4,F10.0)
    1 FORMAT (3F10.2)
    2 FORMAT (3F10.2)
    3 FORMAT (3E15.1)
    4 FORMAT ( E10.2)
      STOP
      END
$ENTRY
   4000.00      11.          2.
     66.00     200.00    1000.00
     1000.0E-12       200.0E-12        50.0E-12
  2.00E-06
$IBSYS
```

APPENDIX D

For T.M. Waves (Figure 4-1)

$$\nabla^2_{xy} E_z(x,y) = -(\gamma^2 + k_o^2) E_z(x,y)$$

$$\frac{\partial^2 E_z(x,y)}{\partial x^2} + \frac{\partial^2 E_z(x,y)}{\partial y^2} = -(\gamma^2 + k_o^2) E_z(x,y)$$

Assume that the solution may be written as a product of two terms, one a function of x only, the other a function of y only;

$$E_z(x,y) = XY$$

so $$\frac{1}{X}\frac{\partial^2 X}{\partial x^2} + \frac{1}{Y}\frac{\partial^2 Y}{\partial y^2} = -(\gamma^2 + k_o^2)$$

let $$\frac{1}{Y}\frac{\partial^2 Y}{\partial y^2} = -h_y^2$$

$\therefore$ $$Y = Y_1 \cos(h_y y) + Y_2 \sin(h_y y)$$

let $$h_x^2 = \gamma^2 + k_o^2 - h_y^2$$

$$\frac{1}{X}\frac{\partial^2 X}{\partial x^2} = -h_x^2$$

$$X = X_1 \cos(h_x x) + X_2 \sin(h_x x)$$

$$E_z(x,y) = (X_1 \cos h_x x + X_2 \sin h_x x)(Y_1 \cos h_y y + Y_2 \sin h_y y)$$

boundary conditions

$y = 0, \quad E_z(x,y) = 0 \qquad A = 0$

$$E_z(x,y) = (X_1' \cos h_x x + X_2' \sin h_x x \sin) h_y Y$$

$y = b, \quad E_z(x,y) = 0 \qquad h_y = n\pi/b$

$$E_z(x,y) = (X_1' \cos h_x x + X_2' \sin h_x x) \sin (n\pi/b)\, y$$

for $0 \leq X \leq d$

$x = 0, \quad E_{z1}(x,y) = 0 \qquad X_1' = 0$

$$E_{z1}(x,y) = A_1 \sin h_x x \sin (n\pi/b)\, y$$

or $$E_{z1} = A_1 \sin h_x x \sin (n\pi/b)\, y \; e^{-\gamma z}$$

for $d \leq x \leq a$

$x = a, \quad E_{z2}(x,y) = 0$

$$X_1' \cos h_x a + X_2' \sin h_x a = 0$$

$$X_1' = - \frac{\sin h_x a}{\cos h_x a} X_2'$$

$$E_{z2}(x,y) = X_2'(\sin h_x x - \frac{\sin h_x a}{\cos h_x a} \cos h_x x) \sin (n\pi/b)\, y$$

$$= A_2 \sin h_x(a - x) \sin (n\pi/b)\, y$$

or $$E_{z2} = A_2 \sin h_x(a - x) \sin (n\pi/b)\, y \cdot e^{-\gamma z}$$

where $h_x = \frac{u + jv}{a}$ = complex wave number in the x-direction.

APPENDIX E

The curl equations assuming a time function $e^{j\omega t}$ are

$$\nabla \times \bar{E} = - j\omega\mu_o \bar{H} \qquad \nabla \times \bar{H} = j\omega\varepsilon_o \bar{E}$$

or

$$\frac{\partial E_z}{\partial y} + \gamma E_y = -j\omega\mu_o H_x \qquad \frac{\partial H_z}{\partial y} + \gamma H_y = j\omega\varepsilon_o E_x$$

$$-\gamma E_x - \frac{\partial E_z}{\partial x} = - j\omega\mu_o H_y \qquad -\gamma H_x - \frac{\partial H_z}{\partial x} = j\omega\varepsilon_o E_y$$

$$\frac{\partial E_y}{\partial x} - \frac{\partial E_x}{\partial y} = -j\omega\mu_o H_z \qquad \frac{\partial H_y}{\partial x} - \frac{\partial H_x}{\partial y} = j\omega\varepsilon_o E_z$$

From the above equations, E_x, E_y, H_x and H_y can be represented in terms of E_z and H_z.

$$E_x = \frac{-1}{\gamma^2 + k_o^2} \left(\gamma \frac{\partial E_z}{\partial x} + j\omega\mu_o \frac{\partial H_z}{\partial y} \right)$$

$$E_y = \frac{1}{\gamma^2 + k_o^2} \left(-\gamma \frac{\partial E_z}{\partial y} + j\omega\mu_o \frac{\partial H_z}{\partial x} \right)$$

$$H_x = \frac{1}{\gamma^2 + k_o^2} \left(j\omega\varepsilon_o \frac{\partial E_z}{\partial y} - \gamma \frac{\partial H_z}{\partial x} \right)$$

$$H_y = \frac{-1}{\gamma^2 + k_o^2} \left(j\omega\varepsilon_o \frac{\partial E_y}{\partial x} + \frac{\partial H_z}{\partial y} \right)$$

From Appendix D, for $0 \leq x \leq d$

$$E_{zl} = A_1 \sin h_x x \sin (n\pi/b)\, y \; e^{-\gamma z}$$

$$\therefore \quad \frac{\partial E_{zl}}{\partial x} = h_x A_1 \cos h_x x \sin (n\pi/b)\, y \; e^{-\gamma z}$$

$$\frac{\partial E_{zl}}{\partial y} = (n\pi/b)\, A_1 \sin h_x x \cos (n\pi/b)\, y \; e^{-\gamma z}$$

and

$$H_{zl} = B_1 \cos h_x x \cos (n\pi/b)\, y \; e^{-\gamma z}$$

$$\therefore \quad \frac{\partial H_{zl}}{\partial x} = -h_x B_1 \sin h_x x \cos (n\pi/b)\, y \; e^{-\gamma z}$$

$$\frac{\partial H_{zl}}{\partial y} = -(n\pi/b)\, B_1 \cos h_x x \sin (n\pi/b)\, y \; e^{-\gamma z}$$

so

$$E_{xl} = \frac{-1}{\gamma^2 + k_o^2} \left\{ \gamma h_x A_1 - j\omega\mu_o (n\pi/b)\, B_1 \right\} \cos h_x x \sin (n\pi/b)\, y \; e^{-\gamma z}$$

$$E_{yl} = \frac{1}{\gamma^2 + k_o^2} \left\{ -\gamma (n\pi/b)\, A_1 - j\omega\mu_o h_x B_1 \right\} \sin h_x x \cos (n\pi/b)\, y \; e^{-\gamma z}$$

$$E_{zl} = A_1 \sin h_x x \sin (n\pi/b)\, y \; e^{-\gamma z}$$

$$H_{xl} = \frac{1}{\gamma^2 + k_o^2} \left\{ j\omega\varepsilon_o (n\pi/b)\, A_1 + \gamma h_x B_1 \right\} \sin h_x x \cos (n\pi/b)\, y \; e^{-\gamma z}$$

$$H_{yl} = \frac{-1}{\gamma^2 + k_o^2} \left\{ j\omega\varepsilon_o h_x A_1 - \gamma (n\pi/b)\, B_1 \right\} \cos h_x x \sin (n\pi/b)\, y \; e^{-\gamma z}$$

$$H_{zl} = B_1 \cos h_x x \cos (n\pi/b)\, y \; e^{-\gamma z}$$

Similar for $d \leq x \leq a$

$$E_{x2} = \frac{1}{\gamma^2 + k_o^2} \left[\gamma h_x A_2 + j\omega\mu_o (n\pi/b) B_2\right] \cos h_x(a-x) \sin (n\pi/b)y \, e^{-\gamma z}$$

$$E_{y2} = \frac{1}{\gamma^2 + k_o^2} \left[-\gamma (n\pi/b) A_2 + j\omega\mu_o h_x B_2\right] \sin h_x(a-x) \cos (n\pi/b)y \, e^{-\gamma z}$$

$$E_{z2} = A_2 \sin h_x(a-x) \sin (n\pi/b) y \; e^{-\gamma z}$$

$$H_{x2} = \frac{1}{\gamma^2 + k_o^2} \left[j\omega\varepsilon_o (n\pi/b) A_2 - \gamma h_x B_2\right] \sin h_x(a-x) \cos (n\pi/b)y \, e^{-\gamma z}$$

$$H_{y2} = \frac{1}{\gamma^2 + k_o^2} \left[j\omega\varepsilon_o h_x A_2 + \gamma (n\pi/b) B_2\right] \cos h_x(a-x) \sin (n\pi/b)y \, e^{-\gamma z}$$

$$H_{z2} = B_2 \cos h_x(a-x) \cos (n\pi/b) y \; e^{-\gamma z}$$

for L.S.E. waves $E_{x1} = E_{x2} = 0$

$$\frac{B_1}{A_1} = \frac{B_2}{A_2} = \frac{\gamma h_x}{j\omega\mu_o h_y}$$

for L.S.M. waves $H_{x1} = H_{x2} = 0$

$$\frac{B_1}{A_1} = \frac{B_2}{A_2} = \frac{j\omega\varepsilon_o h_y}{\gamma h_x}$$

APPENDIX F

IBM 7040 Computer Programme II

Numerical calculation of the theoretical solution for the complex propagation constant ($\gamma = \alpha + j\beta$) of a film-loaded waveguide in Chapter I.

$$\frac{u \sin h\, v - v \sin u}{\cosh v - \cos u} = \frac{\omega \mu_o a}{2R}$$

$$\frac{u \sin u + v \sinh v}{\cosh v - \cos u} = \frac{\omega \mu_o a}{2} (\omega \varepsilon_r c_o t_f)$$

$$(\alpha + j\beta)^2 = \left[\frac{u + jv}{a}\right]^2 - \omega^2 \mu_o \varepsilon_o$$

```
$JOB          003501 CHAN T.          020    005
$IBJOB        NODECK
$IBFTC
C       MICROWAVE CIRCUIT
        DIMENSION R(50),AA(50)
        READ 1, U,V,EPS1,EPS2
        READ 2, W,UO,EO,A
        READ 3,(R(J),J=1,8)
        PRINT 5, U,V,EPS1,EPS2
        PRINT 5, W,UO,EO,A
        EPS3=0.004
        DO 600 I=1,8
        AA(I)=(W*UO*A)/(R(I)*2.)
  100   COSHU=(EXP(U)+EXP(-U))/2.
        SINHU=(EXP(U)-EXP(-U))/2.
        COSHV=(EXP(V)+EXP(-V))/2.
        SINHV=(EXP(V)-EXP(-V))/2.
        F=U*SIN(U)+V*SINHV-EPS3*(COSHV-COS(U))
        G=V*SIN(U)-U*SINHV+AA(I)*(COSHV-COS(U))
        FU=U*COS(U)+SIN(U)+EPS3*SIN(U)
        FV=V*COSHV+SINHV+EPS3*SINHV
        GU=V*COS(U)-SINHV+AA(I)*SIN(U)
        GV=SIN(U)-U*COSHV+AA(I)*SINHV
        B=(FV*G-GV*F)/(FU*GV-FV*GU)
        C=(GU*F-FU*G)/(FU*GV-FV*GU)
        XX=U+B
        YY=V+C
        IF (ABS(U-XX).GT.EPS1) GO TO 200
        IF (ABS(V-YY).GT.EPS2) GO TO 200
        GO TO 300
  200   U=XX
        V=YY
        GO TO 100
  300   RE=(W**2)*UO*EO-(U**2-V**2)/(A**2)
        RI=(2.*U*V)/(A**2)
        IF (RE.LT.0.0) GO TO 400
        FI=ATAN(RI/RE)
        GO TO 500
  400   FI=3.14159-ATAN(ABS(RI/RE))
  500   ALPHA=(SQRT(ABS(SQRT(ABS(RE**2+RI**2)))))*SIN(FI/2.)
        BETA=(SQRT(ABS(SQRT(ABS(RE**2+RI**2)))))*COS(FI/2.)
        PRINT 6, R(I),XX,YY
        PRINT 111, RE,RI,FI
        PRINT 222, BETA,ALPHA
  600   CONTINUE
    1   FORMAT (F5.1,F10.4,F5.3,F10.7)
    2   FORMAT (4E20.4)
    3   FORMAT (8F10.1)
    5   FORMAT (10X,4E20.9//)
    6   FORMAT (6H R(I)=,F7.1,4X,6H    U=,F17.8,4X,7H     V=,F20.8)
  111   FORMAT (17X,6H   RE=,F17.8,4X,7H    IM=,F17.8,4X,5H PHI=,F12.8//)
  222   FORMAT (17X,6H BETA=,F17.8,4X,7H ALPHA=,F17.8//)
        STOP
        END
$ENTRY
```

REFERENCES

(1) Arthur, J.B., Gibson, A.F. and Granville, J.W.: "The Effect of High Electric Fields on the Absorption of Germanium at Microwave Frequencies", Journal of Electronics, 2, p. 145,(1956).

(2) Gunn, J.B.: "The Field Dependence of Electron Mobility in Germanium", Journal of Electronics, 2, p. 87,(1956).

(3) Gibson, A.F. and Granville, J.W.: "Infra Red and Microwave Modulators Using Germanium", and "Solid State Phenomena in Electric Circuits", Symposium, Brooklyn Polytechnic Institute, New York, p. 303,(1957).

(4) Gibson, A.F., Granville, J.W. and Paige, E.G.: "A Study of Energy Loss Processes in Germanium at High Electric Fields using Microwave Techniques", J.Phys.Chem.Solids, 19, p. 198,(1961).

(5) Grubbs, W.J.: "Hall Effect Devices", Bell System Technical Journal, 38, p. 853,(1959).

(6) Barlow, H.E.M. and Krishna, K.V.G.: "A Hall-Effect Microwave Mixer", The Institution of Electrical Engineers, p. 131,(March 1962).

(7) Wolfe, W.L. and Ballard, S.S.: "Optical Materials, Films and Filters for Infra-Red Instrumentation", Proceedings of the Institute of Radio Engineers", 47, p. 1540,(1959).

(8) Sondheimer, E.H.: "The mean Free path of Electron in Metals", Advances in Physics, 1, p.1,(1952).

(9) Prior, A.C.: "Electron Mobility in InSb at High Electric Fields", Journal of Electronics and Control, 4, p. 165,(1958).

(10) Glicksman, M. and Steele, M.: "High Electric Field Effects in n-InSb", Physical Review, 110, p. 1204,(1958).

(11) Glaso, G.N. and Lebacqz, J.V.: "Pulse Generators", M.I.T. Radiation Laboratory Series, Vol. 5.

(12) Glaso : loc. cit. p. 177.

(13) Glaso : loc. cit. p. 179.

(14) Gunn, M.W.: "A High Voltage Pulse Generator", Electronic Engineering, p. 824,(Dec., 1962).

(15) Glaso,: loc. cit., p. 14.

(16) Edwards, W.D.; "High Voltage Sawtooth and Rectangular Wave Pulse Generator", Electronic Engineering, p. 36,(Jan., 1954).

(17) Ramo, S. and Whinnery, J.R.: "Fields and waves in Modern Radio", John Wiley and Sons, New York, p. 368, (1953).

(18) Bate, G. and Taylor, K.N.R.: "Production and Properties of Thin Layers of Indium Antimonide", Journal of Applied Physics, 31, p. 991,(1960).

(19) Hannay, N.B.: "Semiconductors", Reinhold, New York, p. 395,(1959).

(20) Paparoditis, C.: "Preparation et quelques proprietes electriques de couches minces de InSb", Comptes Rendus des Seances de l'Academie des Sciences, 245, p. 256, (1957).

(21) Dale, E.B. and Senecal, G.: "Annealing effects in Evaporated InSb films", Journal of Applied Physics, Vol. 33, N.8, p. 2526, (1962).

(22) Kurov, G.A. and Pinsker, Z.G.: "Structure and properties of films produced by the vacuum evaporation of InSb", Soviet Phys - Tech. Phy. 3, p. 26, (1958).

(23) Launey, J.: "Effect Hall et magnetoresistance d'indium des lames mince d'antimoniure", Comptes Rendus des Seances de l'academie des Sciences, 245, p. 1122, (1957).

(24) Launey, J. and Colombani, A.: "Resultats theoriques concernant les couches minces d'antimoniure d'indium", Comptes Rendus des Seances de l'academie des Sciences, 245, p. 1607, (1957).

(25) Presnov, V.A. and Sinorov, V.F.: "The production of Investigation of Intermetallic Compounds in Thin Films", Soviet Physics - Technical Physics, 2, p. 104, (1957).

(26) Günther, K.G.: "Aufdampfschichten halbleitenden III-V-Verbindungen", Naturforsch, 13a, p. 1081,(1958).

(27) Koike, R. and Barlow, H.E.M.: "Microwave Measurements on the Magneto-Resistance Effect in Semiconductors", The Institution of Electrical Engineers, p. 137, (March, 1962).

(28) Holland, L.: "Vacuum Deposition of thin films", John Wiley and Sons, New York, p. 145,(1961).

(29) Montgomery, C.G.: "Technique of microwave measurements", M.I.T. Radiation Laboratory Series, Vol. 11, p. 35.

(30) Montgomery,: loc. cit., p. 27.

(31) Smith, R.A.: "Semiconductors", C.U.P., England, p. 393,(1959).

(32) Collin, R.E.: "Field Theory of Guided Waves, McGraw-Hill, New York, p. 225,(1960).

(33) Pincherle, L.: "Electromagnetic Waves in Metal Tubes Filled Longitudinally with two Dielectrics", Physical Review, Vol. 66, p. 118, (Sept. 1944).

(34) Harrington, R.F.: "Time-Harmonic Electromagnetic fields", McGraw-Hill, New York, p. 154,(1961).

(35) Ramo,: loc. cit.

(36) Shockley, W.: "Electrons and Holes in Semiconductors", D. Van Nostrand, New York,(1963).